JCI The Journal of Clinical Investigation

Breast cancer derived GM-CSF regulates arginase 1 in myeloid cells to promote an immunosuppressive microenvironment

Xinming Su, … , Samuel Achilefu, Katherine N. Weilbaecher

J Clin Invest. 2021. https://doi.org/10.1172/JCI145296.

Research In-Press Preview Immunology Oncology

Graphical abstract

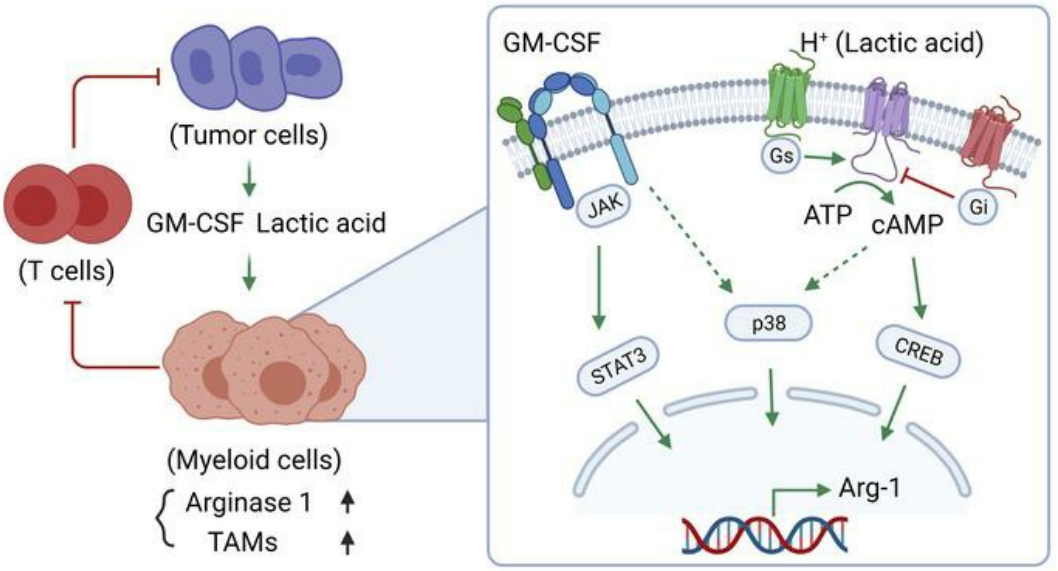

Title:

Breast cancer derived GM-CSF regulates arginase 1 in myeloid cells to promote an immunosuppressive microenvironment

Xinming Su[1], Yalin Xu[1], Gregory C. Fox[1], Jingyu Xiang[1], Kristin A. Kwakwa[1], Jennifer L. Davis[1], Jad I. Belle[1], Wen-Chih Lee[2], Wing Hing Wong[1,3], Francesca Fontana[1], Leonel F. Hernandez-Aya[1], Takayuki Kobayashi[1], Helen Tomasson[1], Junyi Su[1], Suzanne J. Bakewell[1], Sheila A. Stewart[1,4,5], Christopher Egbulefu[6], Partha Karmakar[6], Melisa Meyer[1], Deborah J. Veis[1,7,8], David G. DeNardo[1,5,8], Gregory M. Lanza[1], Samuel Achilefu[1,6], Katherine N. Weilbaecher[1,4,5,8*]

[1]Department of Medicine, Washington University School of Medicine, St. Louis, MO 63110, USA
[2]Department of Orthopedic Surgery, Washington University School of Medicine, St. Louis, MO 63110, USA
[3]Edison Family Center for Genome Sciences and Systems Biology, Washington University School of Medicine, St. Louis, MO, 63110, USA
[4]Department of Cell Biology and Physiology, Washington University School of Medicine, St. Louis, MO, 63110, USA
[5]Siteman Cancer Center, Washington University School of Medicine, St. Louis, MO 63110, USA
[6]Department of Radiology, Washington University School of Medicine, St. Louis, MO, 63110, USA
[7]Musculoskeletal Research Center, Histology and Morphometry Core, Washington University School of Medicine, St. Louis, MO, 63110, USA
[8]Department of Pathology and Immunology, Washington University School of Medicine, St. Louis, MO 63110, USA.

***Corresponding author:**
Katherine N. Weilbaecher, MD
Washington University School of Medicine
Campus Box 8069
660 South Euclid Avenue
St. Louis, MO 63110
Phone: (314) 454-8858
Fax: (314) 454-7086
Email: kweilbae@wustl.edu

Conflict of interest: The authors have declared that no conflict of interest exists.

Abstract

Tumor-infiltrating myeloid cells contribute to the development of the immunosuppressive tumor microenvironment. Myeloid cell expression of arginase 1 (Arg-1) promotes a protumor phenotype by inhibiting T cell function and depleting extracellular L-arginine, but the mechanism underlying this expression, especially in breast cancer, is poorly understood. In breast cancer clinical samples and in our mouse models, we identified tumor derived GM-CSF as the primary regulator of myeloid cell Arg-1 expression and local immune suppression through a gene knockout screen of breast tumor cell-produced factors. The induction of myeloid cell Arg-1 required GM-CSF and a low pH environment. GM-CSF signaling through STAT3, p38 MAPK, and acid signaling through cAMP were required to activate myeloid cell Arg-1 expression in a STAT6 independent manner. Importantly, breast tumor cell-derived GM-CSF promoted tumor progression by inhibiting host anti-tumor immunity, driving a significant accumulation of Arg-1 expressing myeloid cells compared to lung and melanoma tumors with minimal GM-CSF expression. Blockade of tumoral GM-CSF enhanced the efficacy of tumor-specific adoptive T-cell therapy and immune checkpoint blockade. Taken together, breast tumor cell-derived GM-CSF contributes to the development of the immunosuppressive breast cancer microenvironment by regulating myeloid cell Arg-1 expression and can be targeted to enhance breast cancer immunotherapy.

Introduction

Immunotherapy is heralded for its promise in cancer (1). Emerging clinical evidence suggests that the immunosuppressive tumor microenvironment (TME) represents a major obstacle for treatment success against several tumor types, including breast cancer (1-3). Higher rates of tumor-infiltrating lymphocytes (TILs) are associated with an increase in durable response and survival (1, 4-6) and have shown promise as indicators of positive response to immune checkpoint blockade (ICB) treatment (1, 7). However, accumulation of inhibitory cells, such as myeloid-derived suppressor cells (MDSCs) and tumor-associated macrophages (TAMs), as well as metabolic constraints inherent to the TME, are important contributors to T cell dysfunction (2, 3, 8, 9). Thus far, no robust predictive biomarkers for ICB have been established in breast cancer (1).

With tumor progression, a supportive and immunosuppressive TME is developed comprising immune cells, cancer-associated fibroblasts (CAFs), endothelial cells, and stromal cells, all embedded within an extracellular matrix (ECM) (3, 10). Heterogeneous populations of tumor-infiltrating myeloid cells (TIMs) are the most abundant immune-related cells in the TME and include monocytes, tumor-associated neutrophils, tumor-associated dendritic cells (DCs), MDSCs, and TAMs (2, 8, 9). In the TME, TIMs exhibit a diverse range of functional phenotypes from antitumor to protumor (2, 8, 9). TAMs, for example, are often broadly divided into one of two categories: anti-tumorigenic or “M1” TAMs, which express high levels of tumor necrosis factor (TNF), inducible nitric oxide synthase (iNOS, or NOS2), and MHC class II molecules; and pro-tumorigenic or “M2” TAMs, which express high levels of arginase 1 (Arg-1), IL-10, and CD206 (2). In many cancer types, including breast cancer, TIMs often exhibit a protumor phenotype in the TME, where they promote tumor growth and metastasis and are associated with poor prognosis in cancer patients (2, 11-13). Indeed, protumor TIMs, especially M2 TAM subsets, can directly inhibit cytotoxic T lymphocyte (CTL) function through at least three distinct mechanisms, including direct cell-cell contact inhibition through checkpoint inhibitory molecules such as PD-L1, production of inhibitory cytokines like IL-10 and TGF-β, and modulation of the metabolic environment through depletion of L-arginine and production of reactive oxygen species (ROS) (2, 3).

Breast cancer tissue is usually infiltrated with a high number of myeloid cells (2, 13), and the presence of abundant $CD68^+$ myeloid cells with low $CD8^+$ CTL infiltration is negatively correlated with patient survival (13). Breast tumor cell-derived factors, especially members of the colony-stimulating factor (CSF) superfamily such as macrophage (M)-CSF (or CSF1), granulocyte (G)-CSF (or CSF3), and GM-CSF (or CSF2), can directly influence myeloid cell populations, regulating their recruitment, proliferation, and function (2, 9, 11, 12). GM-CSF is expressed by nearly 60% of breast cancer patient tumors (14), and has been shown to activate plasmacytoid predendritic cells (pDC) to promote a regulatory Th2 response and to induce immunosuppressive myeloid cells (14-17).

Arg-1 is a well characterized marker of immunosuppressive myeloid cells, and myeloid cell arginine metabolism regulates both innate and adaptive immunity (18). Compared to NOS2 or Arg-2, Arg-1 expression in macrophages plays a larger role in regulating extracellular L-arginine levels (19). TIM-derived Arg-1 can directly suppress T cell function by depleting L-arginine, inhibiting T cell receptor expression and responses (2, 3, 9, 20). Inhibition of Arg-1 reduces the growth of tumors only in immunocompetent mice (20), and macrophage-specific deletion of *Arg1* in mice improved responses to adoptive cell transfer therapy (21). However, in breast cancer, the role and mechanism of Arg-1 expression is not fully understood.

In this study, we found increased numbers of $Arg\text{-}1^+$ myeloid cells in breast cancer preclinical models and in breast cancer patient tumors compared to lung cancer and melanoma tumors. Using CRISPR/Cas9-mediated gene knockout screening in breast cancer cells, we identified GM-CSF as a critical cytokine regulating myeloid cell Arg-1 expression in the breast cancer TME. We show that GM-CSF promotes primary and metastatic tumor growth through these effects on myeloid cell Arg-1 expression. GM-CSF and the acidic TME were required for TIM Arg-1 expression through JAK/STAT3 and cAMP pathways, respectively. Finally, disruption of tumoral GM-CSF reversed resistance to T-cell therapy and immune checkpoint inhibitors. Our data suggest that breast tumor cell-derived GM-CSF contributes to the development of the immunosuppressive breast cancer TME and can be rationally targeted to enhance breast cancer immune therapy.

Results

Arg-1 expressing myeloid cells accumulate in the breast tumor microenvironment

In breast cancer patients, an abundance of myeloid cells and low T cell infiltration in the tumor tissue is associated with poor outcomes (13). To evaluate myeloid cell and T cell dynamics in the breast cancer TME, we performed FACS analysis of immune populations in an orthotopic model of murine ER^+ luminal B breast cancer, PyMT-BO1-GFP-Luc (BO1) in syngeneic C57BL/6 mice (22), at several time points during tumor progression. We found that the percentage of $CD4^+$ and $CD8^+$ T cells among total tumor-infiltrating leukocytes decreased over time, while $CD11b^+$ myeloid cells increased. Moreover, the majority of infiltrated TAMs were of the CD206 expressing, pro-tumorigenic "M2" phenotype (Figure 1A and 1B). The murine $ER^-PR^-Her2^-$ "triple-negative" 4T1 breast tumor cell line has also been shown to recruit high levels of M2 polarized macrophages and exhibits reduced levels of infiltrating T cells in syngeneic BALB/c mice (23).

Arg-1 is an established biomarker for pro-tumor "M2" polarized macrophages (2). To track Arg-1 expressing macrophages during tumor development in vivo, we established orthotopic BO1 tumors in Arg-1 reporter mice (YARG), in which an enhanced yellow fluorescent protein (EYFP) is expressed under the control of the Arg-1 promoter without disruption of normal Arg-1 expression (24). We found that the majority of Arg-1 expressing cells in the breast TME were myeloid cells, and that the tumor-infiltrating $CD45^+$ $CD11b^+$ myeloid cell population consistently represented about half of the cells expressing Arg-1 (Figure 1C and 1D). Importantly, Arg-1^+ cells were found in all myeloid cell subpopulations studied (Figure 1E). Further, we found that Arg-1 expressing TIMs were mostly $CCR2^+$, pointing toward a bone marrow origin (25, 26) (Figure 1F). However, we did not observe Arg-1 induction in the spleen or in bone marrow-resident myeloid cells from tumor-bearing mice, suggesting that Arg-1 induction in tumor-infiltrating myeloid cells primarily occurred within the breast TME (Figure S1).

Comparing BO1 breast tumors with subcutaneous B16F10 melanoma or LLC lung tumor tissue in C57BL/6 mice, we found that the number of Arg-1^+ myeloid cells was exceptionally high in murine breast tumor tissue (Figure 1G). IHC staining confirmed high numbers of Arg-1 expressing cells in the murine BO1 and 4T1 breast tumor tissues (Figure S2). By multi-color immunofluorescence, we found that most Arg-1 expressing myeloid cells were located in the tumor core (Figure 1H).

We next evaluated breast cancer, melanoma, and lung cancer tissue from human patients for myeloid cell Arg-1 expression by immunofluorescence staining. All cancer types exhibited infiltrating $CD68^+$ myeloid cells, but breast cancer tissue had a significantly higher number of $CD68^+$ infiltrating cells per tissue area (Figure 2A). Moreover, less than 10% of $CD68^+$ cells in melanoma and lung cancers expressed Arg-1, whereas over 45% of $CD68^+$ cells were Arg-1^+ in breast cancer tissue (Figure 2B). Evaluation of myeloid subsets in the most common breast cancer subtypes (ER^+, $Her2^+$, and triple negative breast cancer- TNBC) showed higher levels of infiltrating $CD68^+$ myeloid cells compared to normal breast tissue (Figure 2C). In contrast to TNBC, the ER^+ and $Her2^+$ breast cancer subsets had similar ratios of $CD68^+$ cells expressing Arg-1 (Figure 2D). When comparing the Arg-1^+ $CD68^+$ cell numbers based on tumor stage, we found that the number of Arg-1^+ $CD68^+$ myeloid cells increased in later stage cancer (Figure 2E).

These data demonstrate that Arg-1 expressing myeloid cells accumulate at high levels in the breast TME in the three major breast cancer subtypes. Our data also suggest that the breast cancer TME has unique properties that drive tumor-infiltrating myeloid cell Arg-1 expression compared to lung or melanoma tumors.

Tumor cell-produced GM-CSF is necessary to induce myeloid cell Arg-1 expression

To test if tumor cells can directly induce myeloid cell Arg-1 expression, we treated bone marrow macrophages (BMMs) with conditioned media (CM) collected from tumor cells. We used BMM because the majority of tumor infiltrating myeloid cells expressed high levels of CCR2, suggestive of an origin in the bone marrow; additionally, they represent an abundant and reliable source of myeloid cells for mechanistic biochemical studies. We found that both BO1 and 4T1 breast tumor cell-derived CM strongly induced Arg-1 expression in BMMs, while CM collected from Lewis lung carcinoma (LLC) or B16F10 melanoma cells did not (Figure 3A). Tumor cell-derived CM had no direct inhibitory effect on T cell proliferation (Figure 3B), prompting us to evaluate the effect of CM from Arg-1^+ macrophages. BMMs were exposed to tumor cell-derived CM for 24 hours and FACS sorted into Arg-1^+ and Arg-1^- $CD11b^+$ populations; CM from these sorted populations was then harvested and added to the T cell proliferation assay. We found that only conditioned media from Arg-1^+ myeloid cells had an inhibitory effect on the proliferation of activated T cells (Figure 3B, sFigure 3).

To identify candidate tumor-derived secreted factors that could promote pro-tumor myeloid cell phenotypes in the TME, we performed gene expression analysis of FACS sorted tumor cells (GFP^+) and tumor-associated macrophages ($CD206^+$) from BO1 mammary fat pad (MFP) tumors. We found that breast tumor cells express many cytokines and growth factor genes and that TAMs from the breast cancer microenvironment express their reciprocal receptors (Figure 3C). We performed a knockout screen of candidate secreted factors in BO1 and 4T1 breast cancer cells using the CRISPR/Cas9 lentiviral vector system. We validated targeted gene knockout and evaluated tumor cell CM from these knockout lines for the ability to induce BMM Arg-1 expression, identifying GM-CSF as a prime candidate (Figure 3D, 3E, sFigure 4). We confirmed that GM-CSF is present in the CM from WT BO1 and 4T1 cell lines, but absent in CM from knockout cell lines, as measured by ELISA. Interestingly, neither B16F10 melanoma cells nor LLC lung cancer cells exhibited detectable GM-CSF in their CM (Figure 3F).

Consistent with knockout studies, pharmacologic blockade of the GM-CSF present in breast cancer cell CM using neutralizing antibodies resulted in decreased Arg-1 mRNA expression in BMMs; likewise, exogenous GM-CSF added to conditioned media from CSF2 knockout breast cancer cells rescued Arg-1 mRNA expression in BMMs (Figure 3G, 3H). We further confirmed the effect of GM-CSF depletion or rescue on Arg-1 expression by FACS using BMMs from YARG mice (Figure 3I).

To evaluate whether GM-CSF can regulate Arg-1 expression in vivo, we injected BO1-WT or BO1-CSF2 knockout breast tumor cells into MFP tissue of YARG mice and evaluated Arg-1 expressing myeloid cells by FACS. We found a significantly lower number of Arg-1 expressing myeloid cells in BO1-CSF2 knockout tumors (Figure 3J).

To evaluate the role of GM-CSF in myeloid cell Arg-1 expression in other tumor types, we directly injected GM-CSF into established B16F10 tumors and found that the number of Arg-1 expressing myeloid cells was significantly increased 24 h after GM-CSF injection (sFigure 5).

To further confirm these results, B16 melanoma and LLC lung cancer cells were engineered to overexpress GM-CSF. Conditioned media from GM-CSF expressing B16 and LLC cells induced Arg-1 expression from BMMs. In vivo, enforced GM-CSF expression yielded cell line-derived tumors with significantly more Arg-1 expressing tumor infiltrating myeloid cells (sFigure 6).

Together, these results demonstrate that tumor cell-produced GM-CSF is necessary to induce myeloid cell Arg-1 expression.

GM-CSF and lactic acid synergistically induce myeloid cell Arg-1 expression

GM-CSF can regulate Arg-1 expression in BMMs, but the mechanism is not clear (27). When BMMs were treated with GM-CSF alone in naive media, the induced Arg-1 mRNA level was surprisingly low compared to the response observed from treatment with BO1 CM (Figure 4A). A similar experiment with YARG BMMs demonstrated minimal Arg-1 reporter gene expression after GM-CSF alone treatment (Figure 4B). By contrast, the addition of GM-CSF to B16F10 or LLC CM, neither of which is sufficient to induce Arg-1, induced Arg-1 mRNA in BMMs to a level comparable to BO1 CM (Figure 4C). These data indicate that GM-CSF requires a tumor-derived secreted co-factor to induce myeloid cell Arg-1 expression.

Our top candidate for such a co-factor was lactic acid (LA), a common component of the TME in multiple cancer types (28) and previously shown to upregulate macrophage Arg-1 expression (29). LA dissociates into lactate and free hydrogen ions, actively acidifying the TME, and the anion lactate can be measured as a surrogate of tumor cell LA production. Conditioned media from BO1, B16F10, and LLC tumor cells had similar concentrations of lactate (10-15 mM) (Figure 4D). As with GM-CSF alone in cell culture media, we found that LA alone induced Arg-1 mRNA expression in BMMs without significant upregulation at the protein level. Testing multiple combinations of GM-CSF and LA at various concentrations, we found that they synergized to generate high-level Arg-1 mRNA expression from BMMs in a dose-dependent manner (Figure 4E). We confirmed induction of protein expression using this combination both by FACS of BMMs from YARG reporter mice and by western blot (Figure 4F and 4G).

Lactate dehydrogenase A (LDHA), lactate dehydrogenase B (LDHB), and monocarboxylate transporter 1 (MCT1) are important for LA production in tumor cells (28). We genetically knocked out these genes in BO1 cells to quantify their lactate production and the media pH and found that *Ldha* knockout cells had decreased lactate production and increased media pH (Figure 4H, I). Compared to CM from WT cancer cells, CM from *Ldha* knockout cells resulted in diminished Arg-1 induction in BMMs (Figure 4J, 4K).

Next, we asked whether the molecule lactate, independent of H^+, could work with GM-CSF to induce myeloid cell Arg-1 expression. Surprisingly, the combination of sodium lactate and GM-

CSF did not induce Arg-1 expression in BMMs (Figure S7), suggesting that acidified culture conditions may play a role in Arg-1 induction. We tested GM-CSF addition to media across a range of pH values from 6 to 7.4 for Arg-1 induction. We found that GM-CSF only induced myeloid cell Arg-1 expression in acidified media (Figure 4L), and that neutralization of acidic tumor conditioned media with sodium bicarbonate ($NaHCO_3$) could block Arg-1 induction (Figure 4M).

Together, these data indicate that breast tumor-derived GM-CSF is necessary, but not sufficient, to induce myeloid cell Arg-1 expression. LA acidification may be functioning as a co-factor that synergistically induces myeloid cell Arg-1 expression along with GM-CSF.

Tumor-derived GM-CSF drives Arg-1 expression through non-canonical signaling pathways

STAT6 signaling is required for macrophage Arg-1 expression induced by IL-4 (12). To test the role of STAT6 signaling in breast tumor-induced macrophage Arg-1 expression, we treated BMMs from WT YARG mice or *Stat6*$^{-/-}$ YARG mice with either IL-4 or BO1 CM and detected reporter gene EYFP expression by FACS. We found that IL-4 induced Arg-1 expression in WT BMMs, but not in *Stat6*$^{-/-}$ BMMs, while BO1 CM induced Arg-1 expression in both WT and *Stat6*$^{-/-}$ BMMs (Figure 5A, 5B). We obtained the same results by qPCR for Arg-1 expression in a parallel experiment (Figure 5C). In vivo, we found that BO1 orthotopic MFP tumors induced Arg-1 expression by TIMs in both WT and *Stat6*$^{-/-}$ mice (Figure 5D-F). These data suggest that STAT6 signaling is dispensable in breast tumor-induced myeloid cell Arg-1 expression.

Classical GM-CSF signaling proceeds through JAK2/STAT5; however, studies have shown that GM-CSF can also activate STAT3, p38 MAPK, MEK, and ERK1/2 signaling pathways (30-32). To evaluate the downstream signaling pathways essential to breast tumor-induced Arg-1 expression in myeloid cells, we pre-treated BMMs from YARG mice with inhibitors of JAK1/2, STAT3, STAT5, p38, MEK, or ERK1/2, then added BO1 CM for 24 hours and analyzed Arg-1 expression by FACS. We found that the clinical JAK1/2 inhibitor, ruxolitinib, completely blocked BO1 CM induced Arg-1 expression; a JAK2 downstream STAT5 inhibitor, meanwhile, had no effect. Both STAT3 and p38 inhibition reduced BO1 CM-induced Arg-1 expression in a dose-dependent manner. The clinically used MEK inhibitor, trabectedin, partially inhibited Arg-1 expression, while ERK1/2 inhibition had no effect (Figure 5G-I, sFigure 8).

These results suggest that tumor-derived GM-CSF drives breast tumor cell-induced myeloid cell Arg-1 expression through non-canonical JAK/STAT3 and p38 MAPK signaling pathways.

Tumor-derived GM-CSF requires cAMP signaling to drive Arg-1 expression

Cells can respond to changes in environmental pH through pH sensing G protein-coupled receptors (GPCRs) (33). GPCR downstream signaling proceeds through the G alpha subunit, which negatively or positively regulates adenylyl cyclase (AC) activity through inhibitory G protein (Gi) or stimulatory G protein (Gs), respectively (34, 35) (Figure 6A). We first used the Gi inhibitor pertussis toxin (PTX) to pre-treat BMMs from YARG mice for 1 hour, then added breast tumor CM for a further 24 hours before analyzing Arg-1 expression by FACS. We found that PTX dose-dependently enhanced Arg-1 expression (Figure 6B). Forskolin, an AC activator, similarly enhanced breast tumor CM-induced BMM Arg-1 expression (Figure 6C). When combined with GM-CSF, forskolin was sufficient to induce Arg-1 expression in BMMs (Figure 6D), suggesting that acidified tumor CM or LA may signal through the cAMP pathway to induce Arg-1 expression in myeloid cells.

AC activation increases intracellular cyclic AMP (cAMP) concentration and regulates many cellular functions through cAMP response element-binding protein (CREB) (35). To test the necessity of cAMP to promote Arg-1 expression, we pre-treated BMMs with either MDL-12, an AC inhibitor, or KG-501, an inhibitor of CREB binding, then added breast tumor CM or GM-CSF in combination with LA to the BMMs. In both conditions, we found a dose-dependent inhibition of Arg-1 expression (Figure 6E, 6F).

Taken together, these results suggest that tumor cell-derived GM-CSF-induced myeloid cell Arg-1 expression requires both cAMP signaling and the JAK/STAT3 signaling pathways (Figure 6G proposed model).

Breast tumor-derived GM-CSF promotes tumor growth through the modulation of host immune cells

To evaluate the functional role of tumor-derived GM-CSF on breast tumor growth in vivo, we inoculated 4T1-WT or 4T1-CSF2KO (GM-CSF knockout) cells into the MFP tissue of BALB/c mice and measured tumor growth by caliper. We found that GM-CSF knockout tumor cells had significantly decreased tumor growth (Figure 7A) in immunocompetent mice. We performed the

same experiment using BO1-WT or BO1-CSF2KO breast cancer cells in C57BL/6 mice and found the same result (Figure 7B). To rule out the effect of genetic differences between CRISPR modified cell lines, we established BO1 orthotopic MFP tumors and pharmacologically inhibited GM-CSF in the tumor microenvironment using a neutralizing anti-GM-CSF antibody. Compared to isotype control antibody treatment, mice receiving anti-GM-CSF antibody had significantly decreased tumor growth in WT C57BL/6 mice (Figure 7C). Importantly, pharmacological or genetic disruption of tumor-derived GM-CSF did not affect tumor growth in immunocompromised NSG mice (Figure 7D-F). These results indicate that tumor-derived GM-CSF promotes tumor growth by modulating host immune responses.

We also tested the role of GM-CSF in a spontaneous tumorigenesis model by crossing *MMTV-PyMT* mice with GM-CSF knockout (*Csf2*$^{-/-}$) mice to generate *Csf2*$^{-/-}$ *MMTV-PyMT* mice and evaluated tumor development. We found that the median time to tumor appearance in WT *MMTV-PyMT* mice was 96 days, while the median time to tumor appearance in *Csf2*$^{-/-}$ *MMTV-PyMT* mice was 130.5 days. We performed immune cell profiling of tumors from these mice (harvested at the same tumor size) and found that tumors from *Csf2*$^{-/-}$ *MMTV-PyMT* mice had decreased ARG1^{+} CD11b^{+} myeloid cells and CD4^{+} T cell infiltration, while CD8^{+} T cells numbers were increased (sFigure 9). These data show that GM-CSF can modulate tumor growth and alter tumor immune profiles in a spontaneous breast cancer model.

It is known that myeloid cells can inhibit T cell function through Arg-1 expression (2, 3, 9, 20), and our in vitro data indicated that bone marrow macrophages exposed to breast tumor-secreted GM-CSF express Arg-1 and inhibit T cell function (Figure 3). This prompted us to evaluate WT and GM-CSF knockout tumor cell growth in myeloid cell-specific Arg-1 knockout mice (*Arg1*$^{fl/fl}$ *LysM-Cre*$^{+/-}$). Interestingly, as with our studies in immunocompromised NSG mice, we found no significant differences in tumor growth in mice lacking Arg-1 in myeloid cells (Figure 7G), suggesting that Arg-1 protein expression in myeloid cells is particularly important for GM-CSF-induced enhancement of tumor growth.

We next evaluated the immune profile of BO1-WT and BO1-CSF2KO tumors in WT mice. We found that in the myeloid cell compartment, total CD45^{+}CD11b^{+} myeloid cell numbers were decreased in BO1-CSF2KO tumors. Among all myeloid cell populations, the number of monocytes,

granulocytes, and monocyte-derived dendritic cells was not significantly different between WT and GM-CSF knockout BO1 tumors; however, the number of TAMs was decreased in BO1-CSF2KO tumors (Figure 7H, sFigure 10). Compared to WT BO1 tumors, TAMs in the BO1-CSF2KO tumors were also less polarized towards an M2 phenotype (Figure 7I). Evaluation of the entire population of tumor-infiltrating $CD45^+$ cells revealed that the percentage of conventional T cells (Tconv, $CD4^+$ $Foxp3^-$), and $CD8^+$ T cells between BO1-WT and BO1-CSF2KO tumors were not significantly different. However, BO1-CSF2KO tumors exhibited higher ratios of memory Tconv ($CD62L^+$ $CD44^+$) and memory $CD8^+$ T cells ($CD3^+$ $CD8^+$ $CD62L^+$ $CD44^+$), with reduced $PD1^+$ $TIM3^+$ $CD8^+$ T cells compared to BO1-WT tumors (Figure 7j, sFigure 11). These data suggest that loss of tumoral GM-CSF may provide a favorable environment for T cells in breast cancer.

To evaluate whether Arg-1 and GM-CSF mRNA expression relates to T-cell phenotypes in human breast cancer samples, we queried the Gene Expression database of Normal and Tumor tissues 2 (GENT2)(36) for correlations between T cell markers and *ARG1* or *CSF2*. Across all breast cancer subtypes, we identified a significant positive correlation between *ARG1* expression and *CSF2* expression. In some breast cancer subtypes, especially in luminal B, *ARG1* or *CSF2* expression negatively correlated with *CD3E* expression (sFigure 12). We also evaluated T cell subset markers (*CD4* and *CD8A*) and markers that reflect T cell function, including *LAG3*, *HAVCR2*, *PDCD1*, and *FOXP3*. We identified that the expression of the regulatory T cell marker *FOXP3*, significantly correlated with *ARG1* and *CSF2* expression across all breast cancer subtypes. In some breast cancer subtypes, we also observed a correlation between *ARG1* or *CSF2* expression with putative markers of T cell exhaustion, but this signal was not robust across all breast cancer subtypes from the current dataset (Supplemental Table 3 and 4). These data suggest that *CSF2* expression correlates with *ARG1* expression in human breast cancer tissue, and that the expression of *CSF2* or *ARG1* may reflect an unfavorable environment for T cell function.

Taken together, tumor-derived GM-CSF modulates tumor-infiltrating host immune cells in a myeloid Arg-1 protein expression-dependent manner, resulting in enhanced tumor growth. Interruption of tumor cell-derived GM-CSF resulted in decreased TAM infiltration and diminished myeloid cell Arg-1 expression, and may enhance the anti-tumor function of infiltrating T cells.

Disruption of tumor cell-produced GM-CSF enhances the efficacy of immune therapy

Because myeloid cells exposed to breast tumor cell-produced GM-CSF suppressed T cell function in vitro and enhanced tumor growth in immunocompetent mice, we hypothesized that blockade of GM-CSF production from breast tumor cells would increase the efficacy of T cell-targeted cancer immune therapy.

We first evaluated the effect of disruption of tumor-derived GM-CSF on the efficacy of adoptive T cell transfer therapy. We used CD45.1^{+} OT-1 TCR-transgenic T cells that are specific for chicken ovalbumin (OVA) epitope SIINFEKL ($OVA_{254-267}$) peptide bound to H-2K^{b} as the source of anti-tumor-specific T cells (37). We genetically modified tumor cell lines to express $OVA_{254-267}$ by a retroviral vector (38), and identified them as B16-OVA, BO1-OVA, BO1-WT-OVA, and BO1-CSF2KO-OVA, respectively. The expression level of SIINFEKL-bound H-2Kb and MHC-I on B16-OVA and BO1-OVA were similar (sFigure 13).

BO1 and mCherry-expressing BO1-OVA cells were cultured together at a 1:1 ratio and exposed to in vitro expanded OT-1 T cells. After 16 hours, BO1-OVA cells without OT-1 T cell treatment retained their population, while in the treatment group, OT-1 T cells effectively killed $OVA_{254-267}$ expressing BO1-OVA cells (Figure 8A). In vivo, adoptively transferred CD45.1^{+} OT-1 T cells effectively inhibited melanoma B16-OVA subcutaneous tumor growth (Figure 8B) but had no effect on breast cancer BO1-WT-OVA MFP tumor growth (Figure 8C). In contrast, OT-1 T cells attenuated the growth of BO1-CSF2KO-OVA MFP tumors lacking GM-CSF gene expression (Figure 8D). These results show that in comparison to B16 melanoma cells, BO1 breast cancer cells are resistant to adoptive T-cell transfer therapy, and this resistance could be overcome by disrupting tumor cell produced GM-CSF.

As bone metastasis is common and often challenging to treat in patients with breast cancer (39), we asked whether disruption of GM-CSF production could enhance adoptive T cell therapy in a murine bone metastasis model. We intracardially injected BO1-WT-OVA and BO1-CSF2KO-OVA tumor cells to establish tumor infiltration into bones and visceral organs in WT C57BL/6 mice and injected OT-1 T cells on day 5, monitoring tumor burden by bioluminescence imaging (BLI). We found that without OT-1 T cell treatment, there was no significant difference in bone tumor burden between WT and GM-CSF knockout tumors; however, with OT-1 T cell treatment, bone tumor burden in GM-CSF knockout bone metastases was significantly lower compared to WT

(Figure 8E). We further evaluated whether pharmacological blockade of GM-CSF with a neutralizing antibody could enhance the efficacy of OT-1 T cell treatment on bone metastases. We found that anti-GM-CSF antibody treatment alone did not significantly decrease bone tumor burden in our experimental metastasis model; however, when combined with OT-1 T cell treatment, neutralization of GM-CSF significantly reduced bone tumor burden (Figure 8F). These data suggest that genetic or pharmacologic disruption of tumor cell-derived GM-CSF in preclinical models of metastasis can enhance the efficacy of tumor-specific adoptive T cell therapy.

Next, we tested this hypothesis in a model of immune checkpoint blockade (ICB) therapy. The most common ICB targets on T cells are cytotoxic T-lymphocyte antigen 4 (CTLA-4) and programmed cell death protein 1 (PD-1) signaling (40). We administered an anti-PD1 antibody and anti-CTLA4 antibody as a combined neoadjuvant therapy in an orthotopic spontaneous metastatic breast cancer model. We established BO1-WT mammary fat pad tumors in C57BL/6J mice and intravenously injected anti-PD1 and anti-CTLA4 antibodies on days 6, 8, and 10, starting when T cells and myeloid cells are present within the TME. When the primary tumor size reached ~1000 mm^3, we surgically removed the tumor and monitored mice for evidence of spontaneous metastases for 4 weeks by BLI. We found that ICB treatment did not significantly change BO1-WT primary tumor growth or the rate of metastasis (Figure 8G-I). However, the same experiment performed with BO1-CSF2KO tumors showed that ICB treatment decreased GM-CSF knockout primary tumor growth in WT mice. Notably, after tumor resection around 1000mm^3, the metastasis rate in the control group was around 40%, whereas no metastases were observed in the ICB treated group (Figure 8 J-L). These data suggest that disruption of tumor cell-derived GM-CSF can enhance the efficacy of neoadjuvant ICB treatment in both the primary and metastatic settings.

Overall, our results implicate GM-CSF as a contributor to the development of immunosuppression in the TME, and suggest that targeting GM-CSF could enhance the efficacy of immune therapy.

Discussion

Arg-1 expression and its effect on myeloid cells has been well reported, but not much is known about the role and regulation of Arg-1 in breast cancer. Here, we identify GM-CSF produced by breast cancer cells as a critical regulator of the immune suppressive TME through effects on Arg-1 expression in pro-tumor immune suppressive myeloid cells. We show that the effect of GM-CSF on Arg-1 expression in myeloid cells is triggered by the acidic TME and requires the JAK/STAT3 and p38 MAPK signaling pathways. Moreover, breast tumor cell-derived GM-CSF promotes tumor progression through inhibition of host anti-tumor immunity in preclinical mouse models of primary and metastatic tumor growth. We also show that blockade of tumoral GM-CSF enhances the efficacy of tumor-specific adoptive T-cell therapy and immune checkpoint blockade. Therefore, targeting GM-CSF or downstream pathways of GM-CSF could be an alternate way to inhibit myeloid cell Arg-1 expression, reduce immunosuppression in the breast cancer TME, and enhance immunotherapy efficacy.

GM-CSF is largely redundant for steady-state myelopoiesis and virtually undetectable in circulation (41), but can be administered systemically to promote neutrophil recovery after cytotoxic chemotherapy (42). Physiologically, GM-CSF exerts most of its effects at the local level during immune responses and inflammation (30). GM-CSF can enhance dendritic cell function to prime T cells (30, 43) and has been used as an immune adjuvant in cancer vaccines (44). In contrast to the anti-tumor effects noted above, several studies have reported that tumor cell-derived GM-CSF can suppress immune responses, enhancing tumor-infiltrating immunosuppressive cells, including TAMs, G-MDSCs, T-regs, and plasmacytoid predendritic cells (14, 45-48), although the mechanism is not fully understood. Importantly, in human breast cancer, higher levels of GM-CSF expression have been correlated with increased metastasis and reduced survival (14-17).

Here, we show that the pro-tumor and immune suppressive effects of breast tumor-derived GM-CSF require the induction of Arg-1 in tumor-infiltrating myeloid cells that are primarily recruited from the bone marrow. Genetic disruption of GM-CSF in both TNBC and luminal B subtype breast cancer lines (4T1 and PyMT-BO1) substantially decreased the percentage of Arg-1^+ myeloid cells in primary tumor tissue but did not completely inhibit Arg-1 expression,

suggesting that host-derived GM-CSF could also contribute to myeloid cell Arg-1 expression in the TME. Multiple cellular sources of GM-CSF have been described, including epithelial cells, endothelial cells, fibroblasts, stromal cells, and hematopoietic cells (30, 31, 49), and future studies using fresh cancer tissue are aimed at delineating sources of local GM-CSF in the breast cancer TME that may contribute to myeloid Arg-1 induction and subsequent immune suppression.

Arg-1 expression is an established marker of pro-tumor myeloid cells, which have been associated with immune suppression and enhanced tumor growth (18-20). Arg-1 metabolizes the semi-essential amino acid L-arginine into urea and L-ornithine, and is required for maintaining normal cell growth, collagen synthesis, and neuronal development, as well as tissue repair from injury (19). In the tumor microenvironment, infiltrating Arg-1 expressing myeloid cells drive immunosuppression by depleting extracellular L-arginine, resulting in blockade of T cell receptor zeta chain synthesis and inhibition of T cell proliferation (20). Culture of T cells in media with reduced L-arginine levels markedly impairs T cell function (20, 50), while the culture of T cells at high levels of L-arginine enhances T cell anti-tumor activity (51). In murine models, treatment of tumor-bearing mice with either L-arginine or Arg-1 inhibitors or knockout of Arg-1 in myeloid cells decreases tumor growth, reduces metastasis, and relieves myeloid cell-mediated immune suppression (29, 52-54). We found that the significant difference in growth between WT and GM-CSF KO breast tumors was eliminated in *Arg1*$^{fl/fl}$ *LysM-Cre*$^{+/-}$ mice, suggesting that the effect of breast tumor-derived GM-CSF on the immune suppressive TME specifically requires Arg-1 expression by myeloid cells.

Overexpression of Arg-1 mRNA is a poor prognostic factor in many cancer types, including neuroblastoma (55), acute myeloid leukemia (AML) (56), ovarian carcinoma (57), and colorectal cancer (58). In breast cancer patients, increased arginase activity in both tumor tissue and blood was reported, though its prognostic utility has not been established (59-61). We found that in both human patient samples and in preclinical cancer models, melanoma and lung tumors had significantly lower levels of Arg-1^{+} myeloid infiltrating cells compared to breast tumors.

We used a gene expression screen of breast tumor secreted factors to identify GM-CSF as a critical factor to promote immune suppressive macrophage polarization. We identified lactic acid as a factor that could combine with GM-CSF to induce myeloid Arg-1 levels in a dose-dependent

manner. Tumor cell metabolic reprogramming can generate high levels of lactic acid in the TME, secreted in the form of lactate and H^+ ions by the MCT transporter. Lactate concentration is therefore often used as a surrogate measure of metabolic acidosis (2, 28). Neither high levels of lactic acid nor GM-CSF alone can induce high-level Arg-1 expression in myeloid cells (Figure 4), suggesting that induction of Arg-1 expression in TIMs might be heavily dependent on local, overlapping gradients of GM-CSF and lactic acid, in addition to other factors yet to be identified. Our screens focused on secreted factors and did not evaluate the impact of direct cell-cell interactions, which likely also play a critical role in sculpting immune suppressive tumor environments. The significance of this highly local, context-dependent Arg-1 expression by TIMs for response to immune therapy in human breast cancer demands further study.

Myeloid cell Arg-1 expression has been shown to be regulated by IL-4 or IL-13 signaling through STAT6 (2, 59), but the STAT6 pathway was dispensable for both breast tumor conditioned media and GM-CSF/lactic acid induced Arg-1 expression (Figure 5). A well-known signaling pathway downstream of GM-CSF is JAK2/STAT5. Inhibition of JAK1/2 by ruxolitinib completely blocked tumoral GM-CSF induced myeloid cell Arg-1 expression; however, the STAT5 inhibitor CAS 285986-31-4 had no effect. Accordingly, we turned to other pathways known to regulate immunosuppressive MDSCs such as STAT3 (62-64), a previously identified target of GM-CSF signaling in human neutrophils (65, 66). Studies have also showed that both STAT3 and p38 MAPK signaling can be regulated by JAK2 (67-69). Indeed, we found that blockade of STAT3 or p38 MAPK signaling abrogates Arg-1 expression in myeloid cells (Figure 5). Further, we found that acid signaling through GPCRs/cAMP pathway was also required for robust Arg-1 induction in combination with GM-CSF signaling (Figure 6). Therefore, our data suggest that GM-CSF signals through the STAT3 and p38 MAPK pathways within an acidified environment, cooperating with signaling through GPPCRs/cAMP to trigger myeloid cell Arg-1 expression.

The immune profile of GM-CSF knockout tumors in this report exhibited two significant differences: decreased percentage of Arg-1^+ myeloid cells and decreased total TAM infiltration (Figure 7). Either or both phenotypes could contribute to the reduced tumor growth phenotype observed in GM-CSF knockout breast tumors. Importantly, GM-CSF disruption restored sensitivity

to immune checkpoint blockade and antigen-specific $CD8^+$ T cell therapy. Thus, tumor cell produced GM-CSF can modulate TIMs and contribute to an immunosuppressive TME.

Enhanced anti-tumor T cell activity is critical in current checkpoint immune therapy (1, 70, 71). The majority of breast cancer clinical trials are focused on TNBC because this subtype has higher numbers of tumor infiltrating lymphocytes (1). However, the overall response rates to checkpoint treatment in breast cancer are much lower compared to other cancer types like melanoma or lung cancer. Numerous mechanisms of immune suppression have been identified in the breast TME, a better understanding of which is clearly required to design rational combination treatments for patients. One major potential reason for the failure of such therapeutic interventions is that tumor cell metabolism can impact the TME to limit immune responses and present barriers to cancer therapy (2, 10, 70, 71). L-arginine is one of the essential nutrients required for proper T cell function that can be depleted by Arg-1 expressing myeloid cells in the TME (19). There are currently no arginase inhibitors available for clinical use due to *in vivo* stability, bioavailability, and safety issues (59, 72). Here, we found that GM-CSF, a cytokine that normally promotes immunity, can induce the immune inhibitory enzyme Arg-1 in acidic microenvironments common across a variety of cancers. We described the mechanisms and highlighted two signaling pathways, GM-CSF and cAMP, which are critical for myeloid Arg-1 induction. We also tested several key molecules, JAK1/2, STAT3, p38, adenylyl cyclase, and CREB, that can be targeted by inhibitors to block Arg-1 expression in vitro. Several clinical inhibitors targeting JAK2, STAT3, and p38 MAPK pathways for cancer treatment are either FDA approved or currently in clinical trials. Future studies are underway to evaluate inhibition of Arg-1 expression using these inhibitors prior to checkpoint therapy in preclinical models.

Together, our data indicate that targeting of tumor cell produced GM-CSF to alter myeloid cell phenotype may alleviate immunosuppression and improve anti-tumor immunity in breast cancer. This finding extends our understanding of the immune suppressive tumor microenvironment and provides a new strategy for circumventing microenvironment-mediated resistance when designing immunotherapy.

Materials and Methods:

Mice

All animal studies were performed according to the guidelines established by the Washington University, Institutional Animal Care and Use Committee (WU IACUC). WT mice (JAX 000664), *LysM-Cre* mice (JAX 004781)(73), Arg-1 reporter mice (YARG, JAX 015857)(24), *Arg1*$^{fl/fl}$ mice (JAX 008817)(74), GM-CSF KO (*Csf2*$^{-/-}$) mice (JAX 026812)(75), OT-1 mice (JAX 003831)(37), CD45.1 mice (JAX 002014), *Stat6*$^{-/-}$ mice (JAX 005977)(76) and *MMTV-PyMT* mice (JAX 022974)(77) are all C57BL/6J background and from the Jackson Laboratory. BALB/c mice (JAX 000651) and NOD SCID gamma (NSG) mice (JAX 005557) are also from the Jackson Laboratory. *Arg1*$^{fl/fl}$ mice were crossed with *LysM-Cre* mice to obtain Arg-1 myeloid cell conditional knockout mice (*Arg1*$^{fl/fl}$ *LysM-Cre*$^{+/-}$). YARG mice were crossed with *Stat6*$^{-/-}$ mice to obtain *Stat6*$^{-/-}$ YARG mice. OT-1 mice were crossed with CD45.1 mice to obtain OT-1-CD45.1 mice. For in vivo experiments, 8 to 12-week-old mice were used. Mice used for in vitro experiments were 6 to 12 weeks old. All mice are housed under pathogen-free conditions according to the guidelines of the WU IACUC.

Cell lines and constructs

The BALB/c background 4T1-FL-GFP murine mammary tumor cell line was originally from Dr. David Piwnica-Worms (The University of Texas, Houston, TX) as previously described (78). The C57BL/6J background PyMT-BO1-GFP-Luc murine mammary tumor cell line was previously reported (22). Both murine breast tumor cell lines had been previously modified to express firefly luciferase and green fluorescent protein. The B16F10-Luc murine melanoma and LLC-Luc murine lung cancer cell lines were provided by Dr. Hodivala-Dilke (UK) (79). Non-labeled B16 and LLC cell lines are from ATCC. Gene knockout cell lines were made using the lentiCRISPR v2 vector system (Addgene 52961), as described (80). All gRNA sequences used for CRISPR knockout experiments are listed in Supplementary Table 1. Virus was packaged using 293T cells and helper plasmids pCMV-DR8.2 and pCMV-VSVG. Tumor cell lines were transduced with viral supernatant for 12 h at 37°C in 6-well tissue culture plates and selected with 5-10 ug/mL puromycin for 3 days. All CRISPR knockout cell lines were validated by ELISA or western blot.

GM-CSF overexpressing B16 and LLC cell lines were established by transfection of plasmid DNA of murine *Csf2* vector pCR3.1-mGM-CSF (Addgene 74465)(81) using lipofectamine 3000 (Thermo

Fisher Scientific) and selected with 1mg/mL G418 for one week. GM-CSF expression from established cell lines (B16-GM and LLC-GM) were confirmed by ELISA.

$OVA_{257-264}$ expressing cell lines were established as described (38). Briefly, HEK293T Phoenix-Ampho cells were transfected with PresentER-SIINFEKL (mCherry) vector (Addgene 102945). After 24 h, cell culture viral supernatant was harvested every 12 h. Tumor cell lines were transduced with viral supernatant for 12 h at 37 degrees in 6-well tissue culture plates. All cell lines were selected with puromycin and purified by FACS sorting according to mCherry expression.

All cell lines were maintained in Dulbecco's Modified Eagle's Medium (DMEM) (Gibco) supplemented with 10% fetal bovine serum (Sigma) and penicillin/streptomycin (Gibco). All cell lines tested negative for mycoplasma.

Mice tumor models

4T1 cells were implanted into BALB/C mice, and PyMT-BO1 cells were implanted into C57BL/6 mice. NSG mice received cell lines from both backgrounds. In vivo orthotopic breast tumor models were established by injection of $1x10^5$ tumor cells, mixed with BD matrigel (BD biosciences) or with PBS in a total of 40 µL, into the fourth mammary fat pad (MFP) tissue of 8-week-old female mice.

For subcutaneous injections, $1x10^6$ tumor cells in 200 µL PBS were injected into the flank of mice. Tumor growth was monitored and measured with digital calipers.

Breast tumor bone metastasis models were established by intracardiac injection with $1x10^5$ tumor cells in 50 µL PBS into 6-week-old mice, as previously described (82). Bioluminescence imaging was used to quantify tumor growth after injection. For antibody treatment, mice were given anti-PD1 and anti-CTLA4 antibodies (2.5mg/kg, Bioxcell) by intravenous injection at the indicated time points. For localized anti-GM-CSF antibody treatment, $1x10^5$ BO1-GFP-Luc breast tumor cells were mixed with matrigel plus either isotype antibody (Control) or anti-GM-CSF antibody before injection into MFP tissue of 8 weeks old female C57BL/6J mice. In metastasis models, anti-GM-CSF antibody (2.5mg/kg, Bioxcell) was administered by intravenous injection at the indicated time points.

For adoptive T cell treatment experiments, OT-1 T cells expanded in vitro before i.v. injection. Briefly, spleen cells from OT-1-CD45.1 mice were harvested and stimulated with 0.5µg/mL OVA peptide and 10 ng/mL IL-2 in T-75 flask, media were refreshed every day with IL-2 for three days.

At day 4, T cells were harvested and $CD8^+$ T cells were purified with MACS CD8α magnetic beads and counted, resuspended in PBS before injection.

In vivo bioluminescence imaging

For bioluminescence imaging of live animals, as previously described (82), mice were injected intraperitoneally with 150 μg/g D-luciferin (Biosynth, Naperville, IL) in PBS, anesthetized with 2.5% isoflurane, and imaged with a charge-coupled device (CCD) camera-based bioluminescence imaging system (IVIS 100; Caliper, Hopkinton, MA; exposure time 1-60 seconds, binning 8, field of view 12, f/stop 1, open filter, anterior side). Signal was displayed as photons/sec/cm^2/sr. Regions of interest (ROI) were defined manually around the legs using Living Image and IgorPro Software (Version 2.50).

Bone marrow macrophage culture and treatment

To generate primary bone marrow macrophages (BMMs), whole bone marrow was extracted from the femurs and tibias of mice, plated in Petri dishes in DMEM containing 10% fetal bovine serum and 50ng/mL M-CSF, and cultured in a 37°C, 5% CO2 incubator. Day 3 cultured BMMs were plated at $5x10^5$ per well in 6-well cell culture plates and treated with GM-CSF (2ng/mL), IL-4 (2ng/mL), or lactic acid (0-20 mM) for 24 h before analysis. Pathway agonist or inhibitors are listed: JAK1/2 inhibitor (Ruxolitinib, Millipore Sigma), STAT3 inhibitor (C188-9, Millipore Sigma), STAT5 Inhibitor (CAS 285986-31-4, Millipore Sigma), MEK inhibitor (Trametinib, Cell Signaling Technology), ERK inhibitor (Ulixertinib, Chemie Tek), P38 MAPK inhibitor (SB203580, AdipoGen), Pertussis toxin (Millipore Sigma), Forskolin (Millipore Sigma), Adenylyl cyclase inhibitor (MDL-12, Millipore Sigma), cAMP-response element-binding protein (CREB) inhibitor (KG-501, Millipore Sigma). All inhibitors were used as pre-treatment 1-2 h before given cytokines or tumor conditioned media. Tumor cell-conditioned media were collected from 24 h cultured tumor cells with a cell density of $5X10^5$ cells per 1mL DMEM media. Tumor conditioned media were 1:1 or 1:2 diluted with fresh media before BMMs treatment. After 24 h or indicated treatment time, cells were detached with DPBS plus 5mM EDTA and directly used for FACS analysis, lysis for western blot, or harvest for qPCR.

Microarray analysis

Microarray was performed with the Genome Technology Access Center at Washington University School of Medicine. The microarray data in this article are available on the GEO

database with accession number GSE75882 (22). PyMT-BO1-GFP-Luc cells and CD206^{hi} TAMs were FACS sorted from day 10 MFP tumor tissue. RNA was isolated from tumor cells and CD206^{hi} TAMs using a Nucleospin RNA II Kit (Clonetech). Data were analyzed as described (22).

Lactate and media pH measurements

Lactate concentration from cell culture conditioned media was measured with L-Lactate Assay Kit I (120001, Eton Bioscience) according to the manufacturer's protocol. Cell culture conditioned media pH was measured by a digital pH meter.

Flow cytometry

Tumor tissues were prepared in single-cell suspension for FACS analysis. Briefly, tumor tissue was manually minced using a scalpel, followed by enzymatic digestion with 1 mg/mL collagenase A (Roche) and DNase I (Sigma-Aldrich) for 30 minutes at 37°C with constant stirring. Cells were filtered through 100 µm nylon strainers (Fisher Scientific), then washed twice in 2% FBS PBS. After counting, 1x10^6 total cells were placed in 200 µL buffer (PBS plus 2% FBS) and incubated for 20 minutes with fluorophore-conjugated anti-mouse antibodies using the manufacturers' recommended concentrations. All antibodies used are listed in Supplementary Table 2. Data acquisition was performed on the LSR-II or X20 system (BD Biosciences), and FlowJo software version 10 (Tree Star) was used for analysis.

Statistics

GraphPad Prism Version 7 (GraphPad Software Inc.) was used for statistical analyses. Differences between groups were evaluated by unpaired 2-tailed Student's t test or 2-way ANOVA for repeated measures. Data are presented as mean ± SEM. *P* values of less than 0.05 were considered statistically significant.

Study approval

Animal work was performed according to the policies of the WU IACUC at Washington University School of Medicine in St. Louis. Mice were analyzed under approved protocols and were provided appropriate care while undergoing research that complied with the standards in the Guide for the Use and Care of Laboratory Animals (National Academies Press, 2011) and the Animal Welfare Act.

Author contributions

XS supervised the project, designed, and performed experiments and wrote the manuscript; XS, YX, GCF, JX, KK, JB, WCL, TK, HT, JS, and MM conducted experiments; XS, YX, GCF, JX, JD, JB, WHW, FF, LHA, and DJV analyzed data; LHA, SJB, SAS, CE, PK, DJV, DD, GL, KK, and SA reviewed and edited the manuscript; KNW supervised the project and designed experiments and reviewed and edited the manuscript.

Acknowledgments

This study was supported by the following grants: NCI P01 CA100730, NCI R01 CA216840, NIH U54CA199092, DoD BCRP W81XWH-16-1-0286, NIAMS R21 AR073507, NIAMS R01 AR070030, and NCI R01CA177670.

The authors thank Drs. Kendall Blumer, Vivek Arora, Brian Van Tine, and Christopher Maher for their valuable expert suggestions and criticism, and Crystal Idleburg, Lynne Collins, and Julie Prior for their expert technical assistance. The authors also thank the Musculoskeletal Research Center for histology (NIH P30-AR057235), the Molecular Imaging Center at Washington University (NIH/NCI P50-CA09056), DDRCC Morphology core (grant # P30 DK52574), The Pat Burkhart Breast Cancer Fund, The Barnes-Jewish Foundation, The St. Louis Men's Group Against Cancer, Washington University MSTP grant (GM07200), and Hope Center Alafi Neuroimaging Lab (NIH Shared Instrumentation grant # S10 RR027552).

References

1. Adams S, Gatti-Mays ME, Kalinsky K, Korde LA, Sharon E, Amiri-Kordestani L, et al. Current Landscape of Immunotherapy in Breast Cancer: A Review. *JAMA Oncol.* 2019.
2. DeNardo DG, and Ruffell B. Macrophages as regulators of tumour immunity and immunotherapy. *Nat Rev Immunol.* 2019;19(6):369-82.
3. Anderson KG, Stromnes IM, and Greenberg PD. Obstacles Posed by the Tumor Microenvironment to T cell Activity: A Case for Synergistic Therapies. *Cancer Cell.* 2017;31(3):311-25.
4. Corredor G, Wang X, Zhou Y, Lu C, Fu P, Syrigos K, et al. Spatial Architecture and Arrangement of Tumor-Infiltrating Lymphocytes for Predicting Likelihood of Recurrence in Early-Stage Non-Small Cell Lung Cancer. *Clin Cancer Res.* 2019;25(5):1526-34.
5. Fu Q, Chen N, Ge C, Li R, Li Z, Zeng B, et al. Prognostic value of tumor-infiltrating lymphocytes in melanoma: a systematic review and meta-analysis. *Oncoimmunology.* 2019;8(7):1593806.
6. Gao G, Wang Z, Qu X, and Zhang Z. Prognostic value of tumor-infiltrating lymphocytes in patients with triple-negative breast cancer: a systematic review and meta-analysis. *BMC Cancer.* 2020;20(1):179.
7. Havel JJ, Chowell D, and Chan TA. The evolving landscape of biomarkers for checkpoint inhibitor immunotherapy. *Nat Rev Cancer.* 2019;19(3):133-50.
8. Awad RM, De Vlaeminck Y, Maebe J, Goyvaerts C, and Breckpot K. Turn Back the TIMe: Targeting Tumor Infiltrating Myeloid Cells to Revert Cancer Progression. *Front Immunol.* 2018;9:1977.
9. Engblom C, Pfirschke C, and Pittet MJ. The role of myeloid cells in cancer therapies. *Nat Rev Cancer.* 2016;16(7):447-62.
10. Hanahan D, and Coussens LM. Accessories to the crime: functions of cells recruited to the tumor microenvironment. *Cancer Cell.* 2012;21(3):309-22.
11. Noy R, and Pollard JW. Tumor-associated macrophages: from mechanisms to therapy. *Immunity.* 2014;41(1):49-61.
12. Lawrence T, and Natoli G. Transcriptional regulation of macrophage polarization: enabling diversity with identity. *Nat Rev Immunol.* 2011;11(11):750-61.
13. DeNardo DG, Brennan DJ, Rexhepaj E, Ruffell B, Shiao SL, Madden SF, et al. Leukocyte complexity predicts breast cancer survival and functionally regulates response to chemotherapy. *Cancer Discov.* 2011;1(1):54-67.
14. Ghirelli C, Reyal F, Jeanmougin M, Zollinger R, Sirven P, Michea P, et al. Breast Cancer Cell-Derived GM-CSF Licenses Regulatory Th2 Induction by Plasmacytoid Predendritic Cells in Aggressive Disease Subtypes. *Cancer Res.* 2015;75(14):2775-87.
15. Burga RA, Thorn M, Point GR, Guha P, Nguyen CT, Licata LA, et al. Liver myeloid-derived suppressor cells expand in response to liver metastases in mice and inhibit the anti-tumor efficacy of anti-CEA CAR-T. *Cancer Immunol Immunother.* 2015;64(7):817-29.
16. Kohanbash G, McKaveney K, Sakaki M, Ueda R, Mintz AH, Amankulor N, et al. GM-CSF promotes the immunosuppressive activity of glioma-infiltrating myeloid cells through interleukin-4 receptor-alpha. *Cancer Res.* 2013;73(21):6413-23.
17. Su S, Liu Q, Chen J, Chen J, Chen F, He C, et al. A positive feedback loop between mesenchymal-like cancer cells and macrophages is essential to breast cancer metastasis. *Cancer Cell.* 2014;25(5):605-20.
18. Rodriguez PC, Ochoa AC, and Al-Khami AA. Arginine Metabolism in Myeloid Cells Shapes Innate and Adaptive Immunity. *Front Immunol.* 2017;8:93.

19. Caldwell RW, Rodriguez PC, Toque HA, Narayanan SP, and Caldwell RB. Arginase: A Multifaceted Enzyme Important in Health and Disease. *Physiol Rev.* 2018;98(2):641-65.
20. Rodriguez PC, Quiceno DG, Zabaleta J, Ortiz B, Zea AH, Piazuelo MB, et al. Arginase I production in the tumor microenvironment by mature myeloid cells inhibits T-cell receptor expression and antigen-specific T-cell responses. *Cancer Res.* 2004;64(16):5839-49.
21. Marigo I, Zilio S, Desantis G, Mlecnik B, Agnellini AHR, Ugel S, et al. T Cell Cancer Therapy Requires CD40-CD40L Activation of Tumor Necrosis Factor and Inducible Nitric-Oxide-Synthase-Producing Dendritic Cells. *Cancer Cell.* 2016;30(3):377-90.
22. Su X, Esser AK, Amend SR, Xiang J, Xu Y, Ross MH, et al. Antagonizing Integrin beta3 Increases Immunosuppression in Cancer. *Cancer Res.* 2016;76(12):3484-95.
23. Allen BM, Hiam KJ, Burnett CE, Venida A, DeBarge R, Tenvooren I, et al. Systemic dysfunction and plasticity of the immune macroenvironment in cancer models. *Nat Med.* 2020;26(7):1125-34.
24. Reese TA, Liang HE, Tager AM, Luster AD, Van Rooijen N, Voehringer D, et al. Chitin induces accumulation in tissue of innate immune cells associated with allergy. *Nature.* 2007;447(7140):92-6.
25. Tsou CL, Peters W, Si Y, Slaymaker S, Aslanian AM, Weisberg SP, et al. Critical roles for CCR2 and MCP-3 in monocyte mobilization from bone marrow and recruitment to inflammatory sites. *J Clin Invest.* 2007;117(4):902-9.
26. Lesokhin AM, Hohl TM, Kitano S, Cortez C, Hirschhorn-Cymerman D, Avogadri F, et al. Monocytic CCR2(+) myeloid-derived suppressor cells promote immune escape by limiting activated CD8 T-cell infiltration into the tumor microenvironment. *Cancer Res.* 2012;72(4):876-86.
27. Jost MM, Ninci E, Meder B, Kempf C, Van Royen N, Hua J, et al. Divergent effects of GM-CSF and TGFbeta1 on bone marrow-derived macrophage arginase-1 activity, MCP-1 expression, and matrix metalloproteinase-12: a potential role during arteriogenesis. *FASEB J.* 2003;17(15):2281-3.
28. Corbet C, and Feron O. Tumour acidosis: from the passenger to the driver's seat. *Nat Rev Cancer.* 2017;17(10):577-93.
29. Colegio OR, Chu NQ, Szabo AL, Chu T, Rhebergen AM, Jairam V, et al. Functional polarization of tumour-associated macrophages by tumour-derived lactic acid. *Nature.* 2014;513(7519):559-63.
30. Becher B, Tugues S, and Greter M. GM-CSF: From Growth Factor to Central Mediator of Tissue Inflammation. *Immunity.* 2016;45(5):963-73.
31. Dougan M, Dranoff G, and Dougan SK. GM-CSF, IL-3, and IL-5 Family of Cytokines: Regulators of Inflammation. *Immunity.* 2019;50(4):796-811.
32. Hansen G, Hercus TR, McClure BJ, Stomski FC, Dottore M, Powell J, et al. The structure of the GM-CSF receptor complex reveals a distinct mode of cytokine receptor activation. *Cell.* 2008;134(3):496-507.
33. Ludwig MG, Vanek M, Guerini D, Gasser JA, Jones CE, Junker U, et al. Proton-sensing G-protein-coupled receptors. *Nature.* 2003;425(6953):93-8.
34. Rosenbaum DM, Rasmussen SG, and Kobilka BK. The structure and function of G-protein-coupled receptors. *Nature.* 2009;459(7245):356-63.
35. Campbell AP, and Smrcka AV. Targeting G protein-coupled receptor signalling by blocking G proteins. *Nat Rev Drug Discov.* 2018;17(11):789-803.
36. Park SJ, Yoon BH, Kim SK, and Kim SY. GENT2: an updated gene expression database for normal and tumor tissues. *BMC Med Genomics.* 2019;12(Suppl 5):101.
37. Hogquist KA, Jameson SC, Heath WR, Howard JL, Bevan MJ, and Carbone FR. T cell receptor antagonist peptides induce positive selection. *Cell.* 1994;76(1):17-27.

38. Gejman RS, Chang AY, Jones HF, DiKun K, Hakimi AA, Schietinger A, et al. Rejection of immunogenic tumor clones is limited by clonal fraction. *Elife.* 2018;7.
39. Weilbaecher KN, Guise TA, and McCauley LK. Cancer to bone: a fatal attraction. *Nat Rev Cancer.* 2011;11(6):411-25.
40. Topalian SL, Drake CG, and Pardoll DM. Immune checkpoint blockade: a common denominator approach to cancer therapy. *Cancer Cell.* 2015;27(4):450-61.
41. Hamilton JA, and Anderson GP. GM-CSF Biology. *Growth Factors.* 2004;22(4):225-31.
42. Mehta HM, Malandra M, and Corey SJ. G-CSF and GM-CSF in Neutropenia. *J Immunol.* 2015;195(4):1341-9.
43. Greter M, Helft J, Chow A, Hashimoto D, Mortha A, Agudo-Cantero J, et al. GM-CSF controls nonlymphoid tissue dendritic cell homeostasis but is dispensable for the differentiation of inflammatory dendritic cells. *Immunity.* 2012;36(6):1031-46.
44. Emens LA, Asquith JM, Leatherman JM, Kobrin BJ, Petrik S, Laiko M, et al. Timed sequential treatment with cyclophosphamide, doxorubicin, and an allogeneic granulocyte-macrophage colony-stimulating factor-secreting breast tumor vaccine: a chemotherapy dose-ranging factorial study of safety and immune activation. *J Clin Oncol.* 2009;27(35):5911-8.
45. Bayne LJ, Beatty GL, Jhala N, Clark CE, Rhim AD, Stanger BZ, et al. Tumor-derived granulocyte-macrophage colony-stimulating factor regulates myeloid inflammation and T cell immunity in pancreatic cancer. *Cancer Cell.* 2012;21(6):822-35.
46. Marigo I, Bosio E, Solito S, Mesa C, Fernandez A, Dolcetti L, et al. Tumor-induced tolerance and immune suppression depend on the C/EBPbeta transcription factor. *Immunity.* 2010;32(6):790-802.
47. Quail DF, Olson OC, Bhardwaj P, Walsh LA, Akkari L, Quick ML, et al. Obesity alters the lung myeloid cell landscape to enhance breast cancer metastasis through IL5 and GM-CSF. *Nat Cell Biol.* 2017;19(8):974-87.
48. Reggiani F, Labanca V, Mancuso P, Rabascio C, Talarico G, Orecchioni S, et al. Adipose Progenitor Cell Secretion of GM-CSF and MMP9 Promotes a Stromal and Immunological Microenvironment That Supports Breast Cancer Progression. *Cancer Res.* 2017;77(18):5169-82.
49. Hamilton JA. GM-CSF in inflammation. *J Exp Med.* 2020;217(1).
50. Bronte V, and Zanovello P. Regulation of immune responses by L-arginine metabolism. *Nat Rev Immunol.* 2005;5(8):641-54.
51. Geiger R, Rieckmann JC, Wolf T, Basso C, Feng Y, Fuhrer T, et al. L-Arginine Modulates T Cell Metabolism and Enhances Survival and Anti-tumor Activity. *Cell.* 2016;167(3):829-42 e13.
52. Miret JJ, Kirschmeier P, Koyama S, Zhu M, Li YY, Naito Y, et al. Suppression of Myeloid Cell Arginase Activity leads to Therapeutic Response in a NSCLC Mouse Model by Activating Anti-Tumor Immunity. *J Immunother Cancer.* 2019;7(1):32.
53. Secondini C, Coquoz O, Spagnuolo L, Spinetti T, Peyvandi S, Ciarloni L, et al. Arginase inhibition suppresses lung metastasis in the 4T1 breast cancer model independently of the immunomodulatory and anti-metastatic effects of VEGFR-2 blockade. *Oncoimmunology.* 2017;6(6):e1316437.
54. Steggerda SM, Bennett MK, Chen J, Emberley E, Huang T, Janes JR, et al. Inhibition of arginase by CB-1158 blocks myeloid cell-mediated immune suppression in the tumor microenvironment. *J Immunother Cancer.* 2017;5(1):101.
55. Mussai F, Egan S, Hunter S, Webber H, Fisher J, Wheat R, et al. Neuroblastoma Arginase Activity Creates an Immunosuppressive Microenvironment That Impairs Autologous and Engineered Immunity. *Cancer Res.* 2015;75(15):3043-53.

56. Mussai F, De Santo C, Abu-Dayyeh I, Booth S, Quek L, McEwen-Smith RM, et al. Acute myeloid leukemia creates an arginase-dependent immunosuppressive microenvironment. *Blood.* 2013;122(5):749-58.
57. Czystowska-Kuzmicz M, Sosnowska A, Nowis D, Ramji K, Szajnik M, Chlebowska-Tuz J, et al. Small extracellular vesicles containing arginase-1 suppress T-cell responses and promote tumor growth in ovarian carcinoma. *Nat Commun.* 2019;10(1):3000.
58. Ma Z, Lian J, Yang M, Wuyang J, Zhao C, Chen W, et al. Overexpression of Arginase-1 is an indicator of poor prognosis in patients with colorectal cancer. *Pathol Res Pract.* 2019;215(6):152383.
59. Grzywa TM, Sosnowska A, Matryba P, Rydzynska Z, Jasinski M, Nowis D, et al. Myeloid Cell-Derived Arginase in Cancer Immune Response. *Front Immunol.* 2020;11:938.
60. de Boniface J, Mao Y, Schmidt-Mende J, Kiessling R, and Poschke I. Expression patterns of the immunomodulatory enzyme arginase 1 in blood, lymph nodes and tumor tissue of early-stage breast cancer patients. *Oncoimmunology.* 2012;1(8):1305-12.
61. Perez G, Olivares IM, Rodriguez MG, Ceballos GM, and Garcia Sanchez JR. Arginase activity in patients with breast cancer: an analysis of plasma, tumors, and its relationship with the presence of the estrogen receptor. *Onkologie.* 2012;35(10):570-4.
62. Chalmin F, Ladoire S, Mignot G, Vincent J, Bruchard M, Remy-Martin JP, et al. Membrane-associated Hsp72 from tumor-derived exosomes mediates STAT3-dependent immunosuppressive function of mouse and human myeloid-derived suppressor cells. *J Clin Invest.* 2010;120(2):457-71.
63. Poschke I, Mougiakakos D, Hansson J, Masucci GV, and Kiessling R. Immature immunosuppressive CD14+HLA-DR-/low cells in melanoma patients are Stat3hi and overexpress CD80, CD83, and DC-sign. *Cancer Res.* 2010;70(11):4335-45.
64. Vasquez-Dunddel D, Pan F, Zeng Q, Gorbounov M, Albesiano E, Fu J, et al. STAT3 regulates arginase-I in myeloid-derived suppressor cells from cancer patients. *J Clin Invest.* 2013;123(4):1580-9.
65. Al-Shami A, Mahanna W, and Naccache PH. Granulocyte-macrophage colony-stimulating factor-activated signaling pathways in human neutrophils. Selective activation of Jak2, Stat3, and Stat5b. *J Biol Chem.* 1998;273(2):1058-63.
66. Brizzi MF, Aronica MG, Rosso A, Bagnara GP, Yarden Y, and Pegoraro L. Granulocyte-macrophage colony-stimulating factor stimulates JAK2 signaling pathway and rapidly activates p93fes, STAT1 p91, and STAT3 p92 in polymorphonuclear leukocytes. *J Biol Chem.* 1996;271(7):3562-7.
67. Rawlings JS, Rosler KM, and Harrison DA. The JAK/STAT signaling pathway. *J Cell Sci.* 2004;117(Pt 8):1281-3.
68. Rebe C, Vegran F, Berger H, and Ghiringhelli F. STAT3 activation: A key factor in tumor immunoescape. *JAKSTAT.* 2013;2(1):e23010.
69. Zhu T, and Lobie PE. Janus kinase 2-dependent activation of p38 mitogen-activated protein kinase by growth hormone. Resultant transcriptional activation of ATF-2 and CHOP, cytoskeletal re-organization and mitogenesis. *J Biol Chem.* 2000;275(3):2103-14.
70. Colligan SH, Tzetzo SL, and Abrams SI. Myeloid-driven mechanisms as barriers to antitumor CD8(+) T cell activity. *Mol Immunol.* 2020;118:165-73.
71. Bader JE, Voss K, and Rathmell JC. Targeting Metabolism to Improve the Tumor Microenvironment for Cancer Immunotherapy. *Mol Cell.* 2020;78(6):1019-33.
72. G SC, van Waarde A, I FA, Domling A, and P HE. Arginase as a Potential Biomarker of Disease Progression: A Molecular Imaging Perspective. *Int J Mol Sci.* 2020;21(15).

73. Clausen BE, Burkhardt C, Reith W, Renkawitz R, and Forster I. Conditional gene targeting in macrophages and granulocytes using LysMcre mice. *Transgenic Res.* 1999;8(4):265-77.
74. El Kasmi KC, Qualls JE, Pesce JT, Smith AM, Thompson RW, Henao-Tamayo M, et al. Toll-like receptor-induced arginase 1 in macrophages thwarts effective immunity against intracellular pathogens. *Nat Immunol.* 2008;9(12):1399-406.
75. Dranoff G, Crawford AD, Sadelain M, Ream B, Rashid A, Bronson RT, et al. Involvement of granulocyte-macrophage colony-stimulating factor in pulmonary homeostasis. *Science.* 1994;264(5159):713-6.
76. Kaplan MH, Schindler U, Smiley ST, and Grusby MJ. Stat6 is required for mediating responses to IL-4 and for development of Th2 cells. *Immunity.* 1996;4(3):313-9.
77. Davie SA, Maglione JE, Manner CK, Young D, Cardiff RD, MacLeod CL, et al. Effects of FVB/NJ and C57Bl/6J strain backgrounds on mammary tumor phenotype in inducible nitric oxide synthase deficient mice. *Transgenic Res.* 2007;16(2):193-201.
78. Smith MC, Luker KE, Garbow JR, Prior JL, Jackson E, Piwnica-Worms D, et al. CXCR4 regulates growth of both primary and metastatic breast cancer. *Cancer Res.* 2004;64(23):8604-12.
79. Baker M, Reynolds LE, Robinson SD, Lees DM, Parsons M, Elia G, et al. Stromal Claudin14-heterozygosity, but not deletion, increases tumour blood leakage without affecting tumour growth. *PLoS One.* 2013;8(5):e62516.
80. Sanjana NE, Shalem O, and Zhang F. Improved vectors and genome-wide libraries for CRISPR screening. *Nat Methods.* 2014;11(8):783-4.
81. Heller L, Pottinger C, Jaroszeski MJ, Gilbert R, and Heller R. In vivo electroporation of plasmids encoding GM-CSF or interleukin-2 into existing B16 melanomas combined with electrochemotherapy induces long-term antitumour immunity. *Melanoma Res.* 2000;10(6):577-83.
82. Su X, Floyd DH, Hughes A, Xiang J, Schneider JG, Uluckan O, et al. The ADP receptor P2RY12 regulates osteoclast function and pathologic bone remodeling. *J Clin Invest.* 2012;122(10):3579-92.

Figure 1

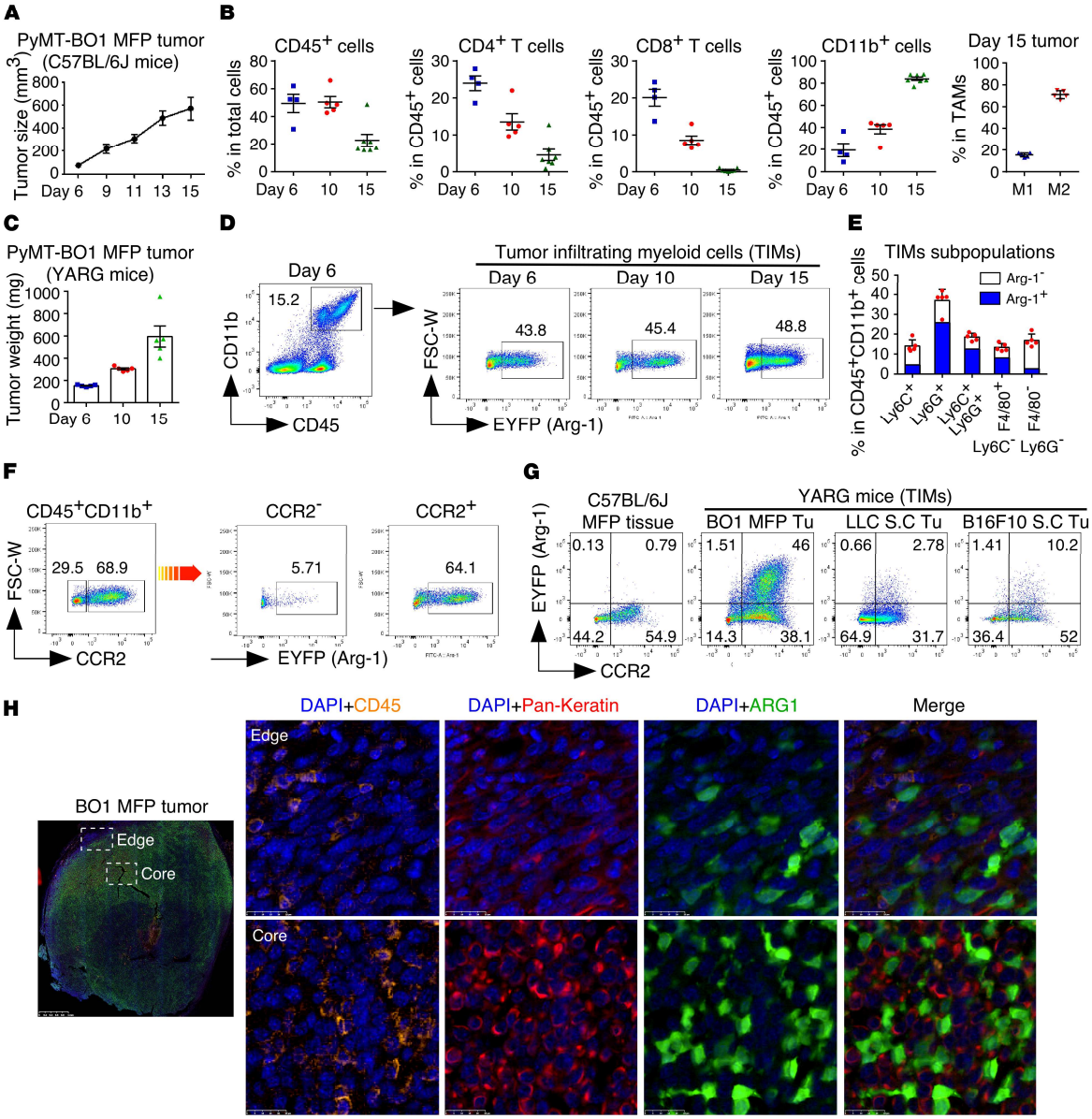
A
PyMT-BO1 MFP tumor (C57BL/6J mice)
Tumor size (mm3)
Day 6 9 11 13 15
B
CD45+ cells
% in total cells
CD4+ T cells
% in CD45+ cells
CD8+ T cells
CD11b+ cells
Day 15 tumor
% in TAMs
M1 M2
C
PyMT-BO1 MFP tumor (YARG mice)
Tumor weight (mg)
D
Day 6
15.2
CD11b
CD45
Tumor infiltrating myeloid cells (TIMs)
Day 6 Day 10 Day 15
43.8 45.4 48.8
FSC-W
EYFP (Arg-1)
E
TIMs subpopulations
% in CD45+CD11b+ cells
Arg-1-
Arg-1+
Ly6C+ Ly6G+ Ly6C+ Ly6G+ F4/80+ F4/80-
Ly6C- Ly6G-
F
CD45+CD11b+
29.5 68.9
FSC-W
CCR2
CCR2-
5.71
CCR2+
64.1
EYFP (Arg-1)
G
C57BL/6J MFP tissue
YARG mice (TIMs)
BO1 MFP Tu
LLC S.C Tu
B16F10 S.C Tu
EYFP (Arg-1)
0.13 0.79 44.2 54.9
1.51 46 14.3 38.1
0.66 2.78 64.9 31.7
1.41 10.2 36.4 52
CCR2
H
DAPI+CD45
DAPI+Pan-Keratin
DAPI+ARG1
Merge
BO1 MFP tumor
Edge
Core

Figure 1. Immunosuppressive Arg-1 expressing myeloid cells accumulated in the breast tumor microenvironment

(A) 1x10^5 PyMT-BO1 breast tumor cells were injected into the MFP tissue of C57BL/6J female mice and tumor growth was measured by digital caliper. **(B)** Single-cell suspensions from whole tumor tissue were analyzed by FACS at day 6, 10 and 15 of tumor growth. The tumor-infiltrating myeloid cell and T cell populations are shown. Tumor-associated macrophages (TAMs) markers are $CD45^+$, $CD11b^+$, $Ly6C^-$, $Ly6G^-$, and $F4/80^+$. M1 TAMs are $MHCII^+$, and M2 TAMs are $CD206^+$. **(C)** Tumor weights from PyMT-BO1 orthotopic tumors in the YARG mice. **(D)** Percentage of Arg-1 expressing myeloid cells in $CD45^+$ $CD11b^+$ tumor-infiltrating myeloid cells (TIMs). **(E)** Percentage of TIM subpopulations in total $CD45^+$ $CD11b^+$ myeloid cells from day 10 tumors. The Arg-1^- cells (white) and Arg-1^+ cells (blue) are labeled in each subpopulation. **(F)** Arg-1 expressing myeloid cells in $CCR2^{hi}$ and $CCR2^{low}$ $CD45^+$ $CD11b^+$ myeloid cells. **(G)** Arg-1 expressing $CD45^+$ $CD11b^+$ myeloid cells in PyMT-BO1 breast cancer MFP tumor tissue, B16F10 melanoma, and LLC lung cancer subcutaneous tumor tissue. **(H)** Immunofluorescent staining of paraffin embedded BO1 MFP tissue. Bar=1 mm (whole tumor tissue), Bar=25 μm (enlarged pictures).

Figure 2

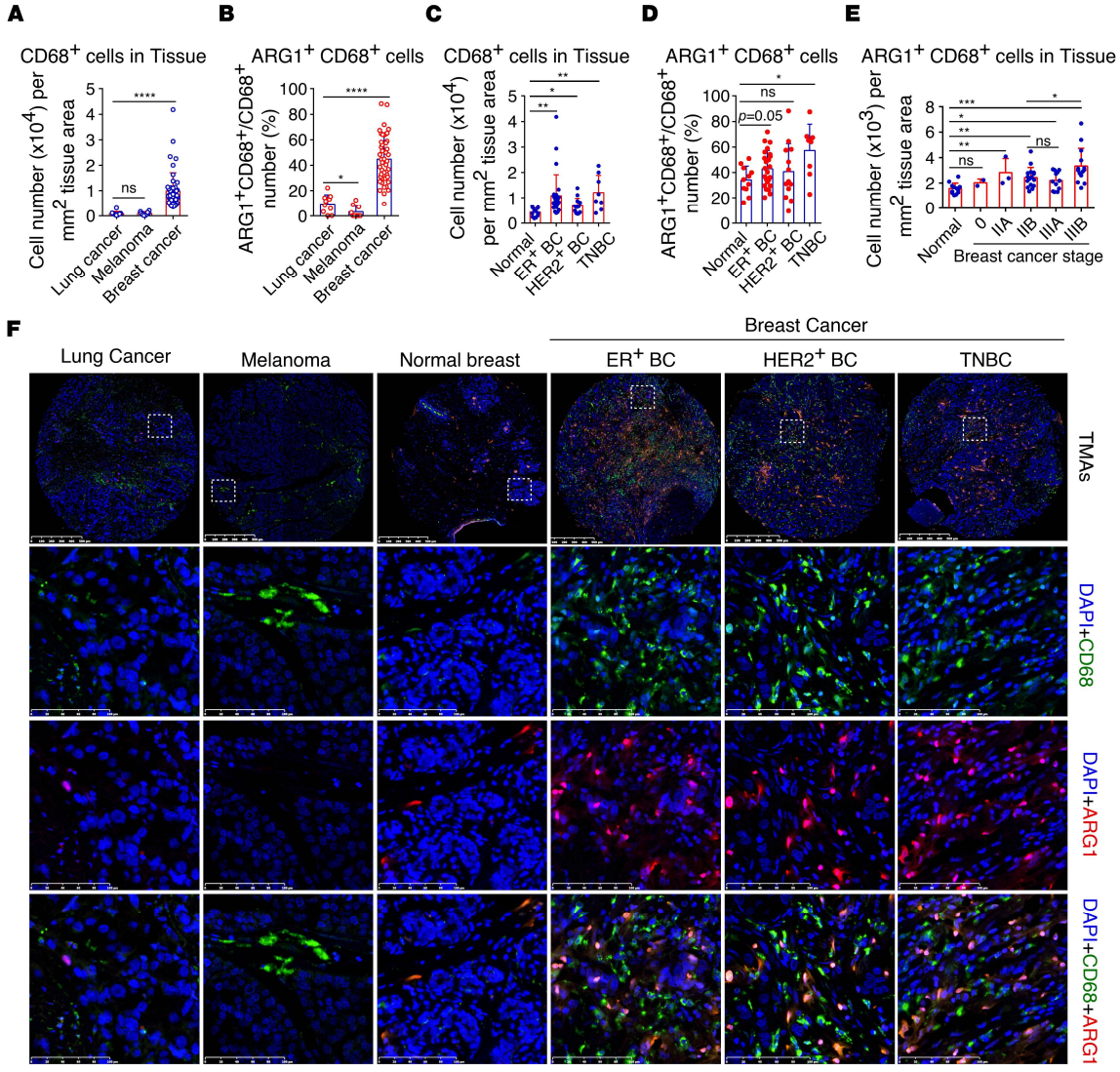
A
CD68+ cells in Tissue
Cell number (x10^4) per mm^2 tissue area
ns
****
Lung cancer
Melanoma
Breast cancer
B
ARG1+ CD68+ cells
ARG1+CD68+/CD68+ number (%)
*
****
Lung cancer
Melanoma
Breast cancer
C
CD68+ cells in Tissue
Cell number (x10^4) per mm^2 tissue area
*
**
**
Normal
ER+ BC
HER2+ BC
TNBC
D
ARG1+ CD68+ cells
ARG1+CD68+/CD68+ number (%)
ns
p=0.05
*
Normal
ER+ BC
HER2+ BC
TNBC
E
ARG1+ CD68+ cells in Tissue
Cell number (x10^3) per mm^2 tissue area
***
*
**
**
ns
ns
*
Normal
0
IIA
IIB
IIIA
IIIB
Breast cancer stage
F
Lung Cancer
Melanoma
Normal breast
Breast Cancer
ER+ BC
HER2+ BC
TNBC
TMAs
DAPI+CD68
DAPI+ARG1
DAPI+CD68+ARG1

Figure 2. Arg-1 expressing myeloid cells accumulated in human breast cancer tissue

Lung cancer (n=10), melanoma (n=10), and breast cancer (n=60) tissue microarrays (TMAs) were used for immunofluorescent staining. **(A)** $CD68^+$ myeloid cell number per mm^2 tissue area, and **(B)** Percentage of $ARG1^+$ cells in total $CD68^+$ cells from lung cancer, melanoma, and breast cancer tissues. **(C)** $CD68^+$ myeloid cell number per mm^2 tissue area, and **(D)** Percentage of $ARG1^+$ cells in total $CD68^+$ cells from breast cancer subtypes. **(E)** $ARG1^+$ $CD68^+$ myeloid cell number per mm2 tissue area from breast cancer based on cancer stage. **(F)** Representative immunofluorescent staining pictures of paraffin-embedded human cancer tissue. Bar=500 μm for whole tissue pictures, Bar=100 μm for enlarged pictures. Data are shown as mean ± SEM, using a two-tailed, unpaired *t*-test with Welch's correction.

Figure 3

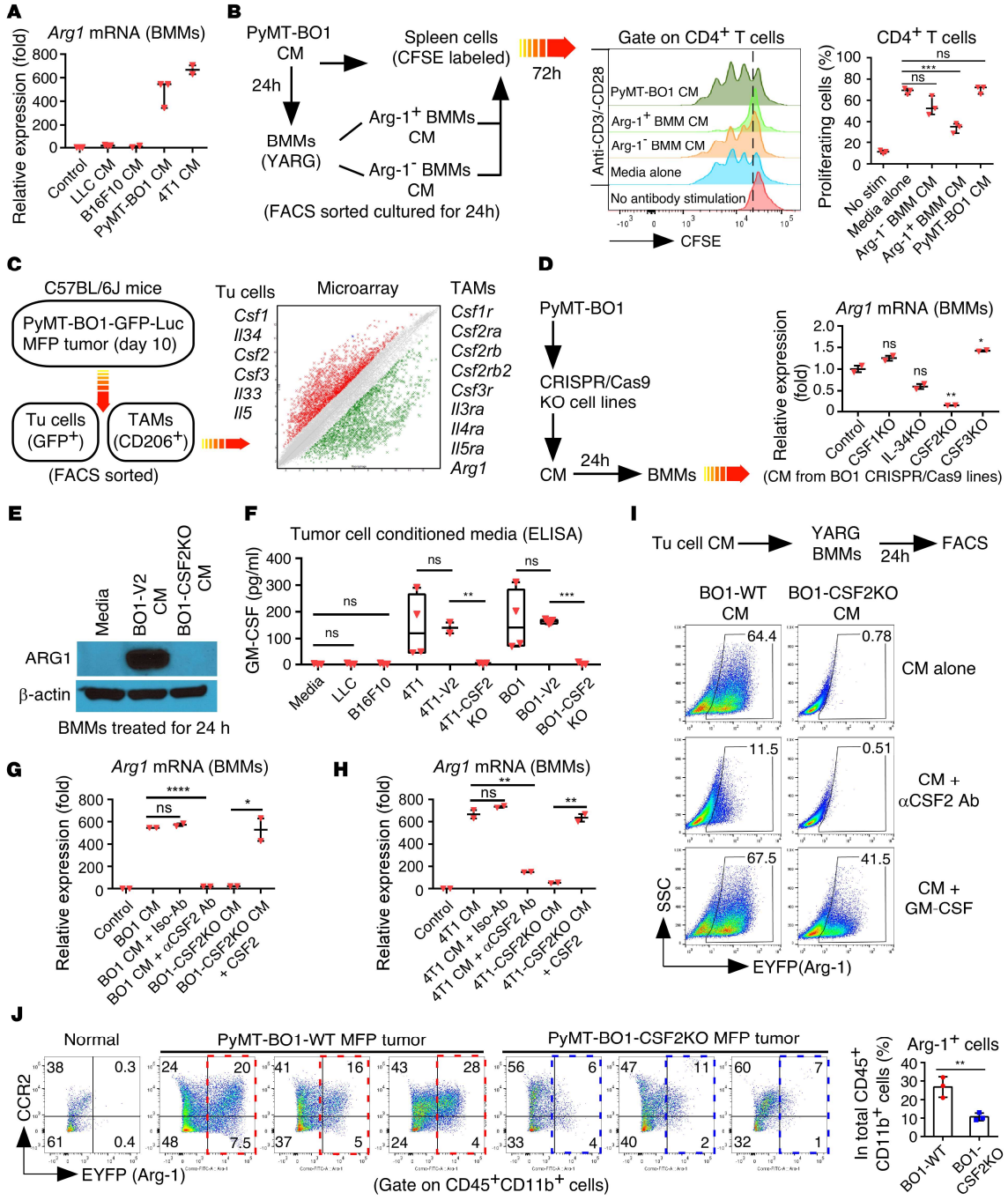
A
Arg1 mRNA (BMMs)
Relative expression (fold)
Control
LLC CM
B16F10 CM
PyMT-BO1 CM
4T1 CM
B
PyMT-BO1 CM
24h
BMMs (YARG)
Arg-1+ BMMs CM
Arg-1- BMMs CM
(FACS sorted cultured for 24h)
Spleen cells (CFSE labeled)
72h
Gate on CD4+ T cells
Anti-CD3/-CD28
PyMT-BO1 CM
Arg-1+ BMM CM
Arg-1- BMM CM
Media alone
No antibody stimulation
CFSE
CD4+ T cells
Proliferating cells (%)
No stim
Media alone
Arg-1- BMM CM
Arg-1+ BMM CM
PyMT-BO1 CM
C
C57BL/6J mice
PyMT-BO1-GFP-Luc MFP tumor (day 10)
Tu cells (GFP+)
TAMs (CD206+)
(FACS sorted)
Tu cells
Microarray
TAMs
Csf1
Il34
Csf2
Csf3
Il33
Il5
Csf1r
Csf2ra
Csf2rb
Csf2rb2
Csf3r
Il3ra
Il4ra
Il5ra
Arg1
D
PyMT-BO1
CRISPR/Cas9 KO cell lines
CM
24h
BMMs
(CM from BO1 CRISPR/Cas9 lines)
Arg1 mRNA (BMMs)
Relative expression (fold)
Control
CSF1KO
IL-34KO
CSF2KO
CSF3KO
E
Media
BO1-V2 CM
BO1-CSF2KO CM
ARG1
β-actin
BMMs treated for 24 h
F
Tumor cell conditioned media (ELISA)
GM-CSF (pg/ml)
Media
LLC
B16F10
4T1
4T1-V2
4T1-CSF2 KO
BO1
BO1-V2
BO1-CSF2 KO
I
Tu cell CM
YARG BMMs
24h
FACS
BO1-WT CM
BO1-CSF2KO CM
64.4
0.78
CM alone
11.5
0.51
CM + αCSF2 Ab
67.5
41.5
CM + GM-CSF
SSC
EYFP(Arg-1)
G
Arg1 mRNA (BMMs)
Relative expression (fold)
Control
BO1 CM
BO1 CM + Iso-Ab
BO1 CM + αCSF2 Ab
BO1-CSF2KO CM
BO1-CSF2KO CM + CSF2
H
Arg1 mRNA (BMMs)
Relative expression (fold)
Control
4T1 CM
4T1 CM + Iso-Ab
4T1 CM + αCSF2 Ab
4T1-CSF2KO CM
4T1-CSF2KO CM + CSF2
J
Normal
PyMT-BO1-WT MFP tumor
PyMT-BO1-CSF2KO MFP tumor
CCR2
EYFP (Arg-1)
(Gate on CD45+CD11b+ cells)
Arg-1+ cells
In total CD45+ CD11b+ cells (%)
BO1-WT
BO1-CSF2KO

Figure 3. Tumor cell produced GM-CSF is necessary to induce myeloid cell Arg-1 expression
(A) *Arg1* mRNA expression from BMMs treated with LLC, B16F10, PyMT-BO1, and 4T1 tumor cell-conditioned media (CM) (*n*=2 or 3). **(B)** CFSE labeled whole spleen cells stimulated with plate-banded anti-CD3E antibody and soluble anti-CD28 antibody, co-cultured with 1:1 diluted CM from PyMT-BO1 or FACS sorted Arg-1^{+} or Arg-1^{-} BMMs pre-treated with PyMT-BO1 CM. T cell proliferation was measured from quantification of CFSE dilution in gated CD4^{+} T cells by FACS (*n*=3). **(C)** Microarray analysis of gene expression from breast tumor cells and CD206^{+} TAMs sorted by FACS from the same tumor tissue. **(D)** *Arg1* mRNA expression in BMMs treated with tumor cell CM from PyMT-BO1 or CRISPR/Cas9 mediated gene knockout PyMT-BO1 tumor cells (*n*=2). **(E)** Western blot of ARG1 from tumor cell CM treated BMMs. **(F)** Quantification of GM-CSF level from tumor cell CM by ELISA (*n*= 2-4). **(G, H)** *Arg1* mRNA expression from BMMs treated with tumor cell CM that included anti-CSF2 antibody or CSF2 (*n*=2). **(I)** Arg-1 expression quantified as EYFP expression by FACS from YARG BMMs treated as indicated. **(J)** 1x10^{5} BO1-WT (vector control) or BO1-CSF2KO breast tumor cells injected into MFP tissue of 8-week-old female YARG mice. At day 10, single-cell suspensions from whole tumor tissue were analyzed by FACS. Arg-1 expression in TIMs is quantified as EYFP expression. In **E** and **I**, data are representative of three independent experiments. Data are shown as mean ± SEM, *p<0.05, **p<0.01, ***p≤0.001, using a two-tailed, unpaired *t*-test with Welch's correction.

Figure 4

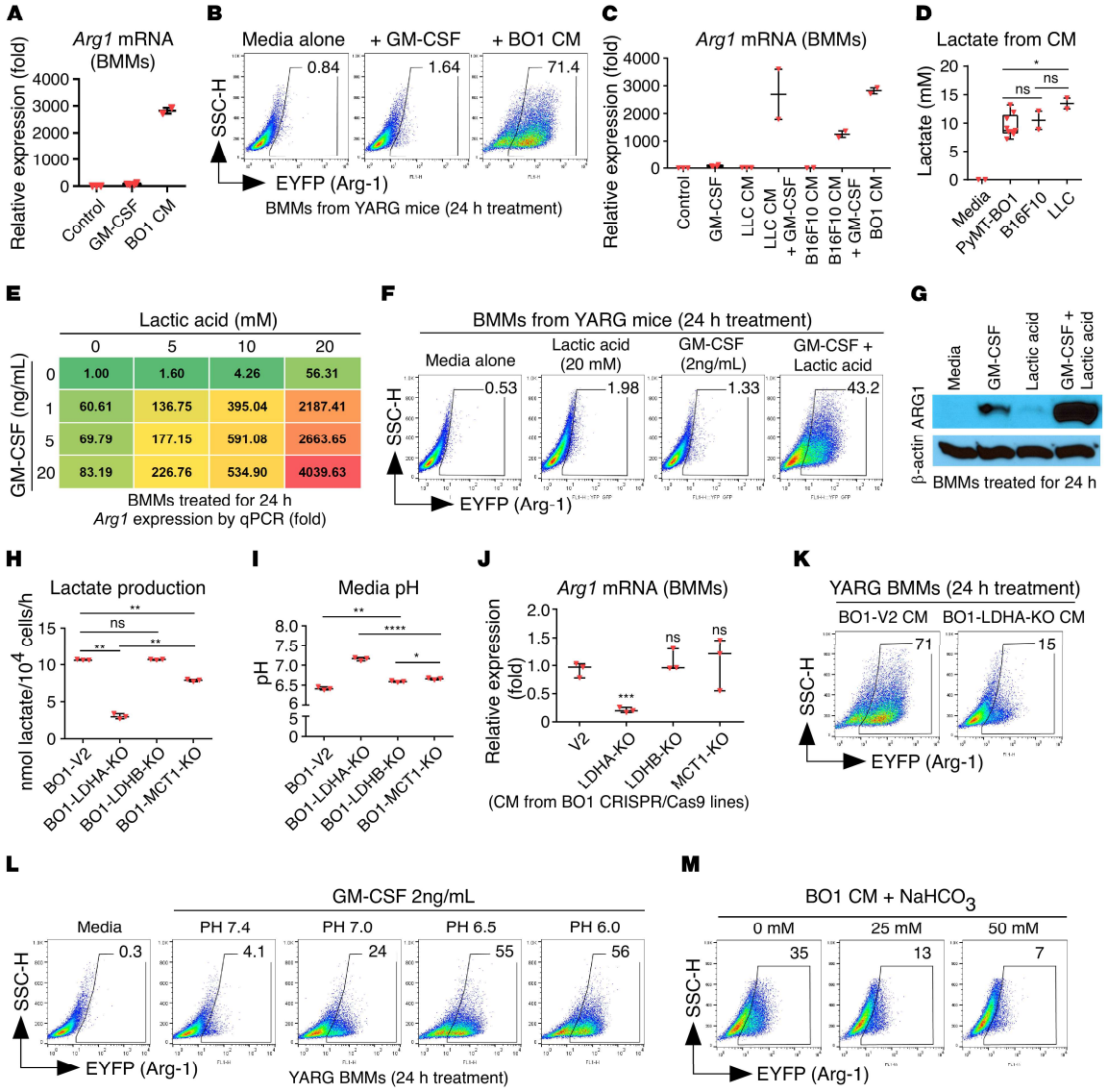
A
Arg1 mRNA (BMMs)
Relative expression (fold)
Control
GM-CSF
BO1 CM
B
Media alone
+ GM-CSF
+ BO1 CM
0.84
1.64
71.4
SSC-H
EYFP (Arg-1)
BMMs from YARG mice (24 h treatment)
C
Arg1 mRNA (BMMs)
Relative expression (fold)
Control
GM-CSF
LLC CM
LLC CM + GM-CSF
B16F10 CM
B16F10 CM + GM-CSF
BO1 CM
D
Lactate from CM
Lactate (mM)
Media
PyMT-BO1
B16F10
LLC
ns
*
E
Lactic acid (mM)
GM-CSF (ng/mL)
1.00
1.60
4.26
56.31
60.61
136.75
395.04
2187.41
69.79
177.15
591.08
2663.65
83.19
226.76
534.90
4039.63
BMMs treated for 24 h
Arg1 expression by qPCR (fold)
F
BMMs from YARG mice (24 h treatment)
Media alone
Lactic acid (20 mM)
GM-CSF (2ng/mL)
GM-CSF + Lactic acid
0.53
1.98
1.33
43.2
SSC-H
EYFP (Arg-1)
G
Media
GM-CSF
Lactic acid
GM-CSF + Lactic acid
β-actin ARG1
BMMs treated for 24 h
H
Lactate production
nmol lactate/10^4 cells/h
BO1-V2
BO1-LDHA-KO
BO1-LDHB-KO
BO1-MCT1-KO
I
Media pH
pH
J
Arg1 mRNA (BMMs)
Relative expression (fold)
V2
LDHA-KO
LDHB-KO
MCT1-KO
(CM from BO1 CRISPR/Cas9 lines)
K
YARG BMMs (24 h treatment)
BO1-V2 CM
BO1-LDHA-KO CM
71
15
SSC-H
EYFP (Arg-1)
L
GM-CSF 2ng/mL
Media
PH 7.4
PH 7.0
PH 6.5
PH 6.0
0.3
4.1
24
55
56
SSC-H
EYFP (Arg-1)
YARG BMMs (24 h treatment)
M
BO1 CM + NaHCO3
0 mM
25 mM
50 mM
35
13
7
SSC-H
EYFP (Arg-1)

Figure 4. GM-CSF and lactic acid synergistically induce myeloid cell arginase 1 expression
(A) *Arg1* mRNA expression from BMMs treated with recombinant GM-CSF or PyMT-BO1 tumor cell CM (*n*=2 or 3). **(B)** $ARG1^+$ cells quantified by FACS from YARG BMMs treated with recombinant GM-CSF or PyMT-BO1 tumor cell CM. **(C)** *Arg1* mRNA expression from BMMs treated with tumor cell CM plus recombinant GM-CSF (*n*=2 or 3). **(D)** Quantification of lactate from tumor cell CM. **(E)** *Arg1* mRNA expression from BMMs treated with recombinant GM-CSF and lactic acid. **(F)** $ARG1^+$ cells quantified by FACS. **(G)** ARG1 expression in BMMs was detected by western blot after GM-CSF and lactic acid treatment. **(H)** Lactate production from tumor cell-conditioned media (*n*=3). **(I)** Tumor conditioned media pH measurement (*n*=3). **(J)** *Arg1* mRNA expression from BMMs (*n*=3). **(K)** $ARG1^+$ cells quantified by FACS. **(L)** YARG BMMs treated with GM-CSF, media pH adjusted with hydrochloric acid (HCL). **(M)** BO1 tumor CM pre-mixed with $NaHCO_3$ as indicated concentration before added to YARG BMMs. In **B, F, G,** and **K-M**, data are representative of three independent experiments. Data are shown as mean ± SEM, **p*<0.05, ***p*<0.01, ****p*≤0.001, using a two-tailed, unpaired *t*-test with Welch's correction.

Figure 5

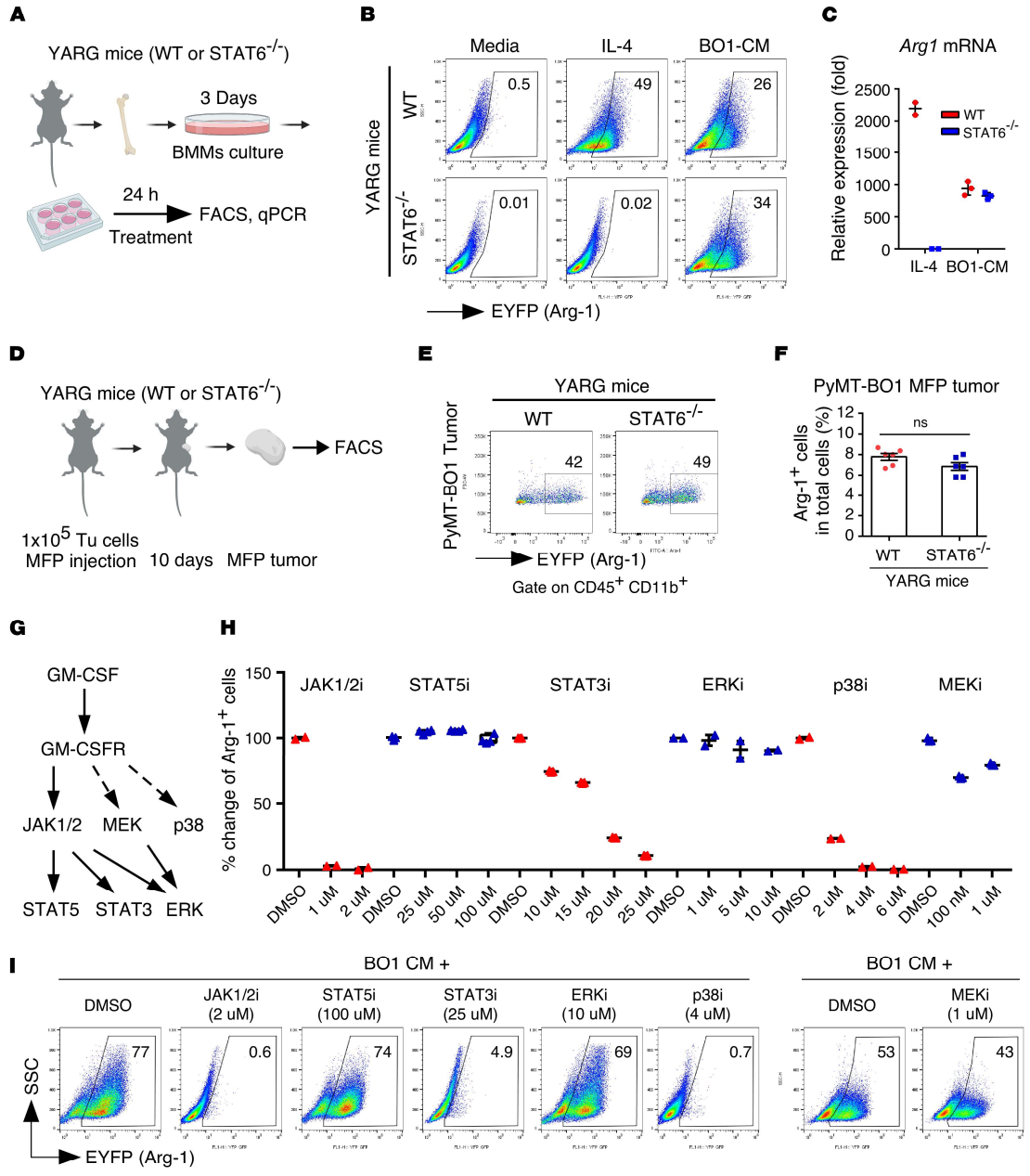
A
YARG mice (WT or STAT6-/-)
3 Days
BMMs culture
24 h
Treatment
FACS, qPCR
B
Media
IL-4
BO1-CM
YARG mice
WT
STAT6-/-
0.5
49
26
0.01
0.02
34
EYFP (Arg-1)
C
Arg1 mRNA
Relative expression (fold)
2500
2000
1500
1000
500
0
WT
STAT6-/-
IL-4
BO1-CM
D
YARG mice (WT or STAT6-/-)
FACS
1x10^5 Tu cells
MFP injection
10 days
MFP tumor
E
YARG mice
WT
STAT6-/-
PyMT-BO1 Tumor
42
49
EYFP (Arg-1)
Gate on CD45+ CD11b+
F
PyMT-BO1 MFP tumor
Arg-1+ cells in total cells (%)
ns
WT
STAT6-/-
YARG mice
G
GM-CSF
GM-CSFR
JAK1/2
MEK
p38
STAT5
STAT3
ERK
H
% change of Arg-1+ cells
JAK1/2i
STAT5i
STAT3i
ERKi
p38i
MEKi
DMSO
1 uM
2 uM
25 uM
50 uM
100 uM
10 uM
15 uM
20 uM
5 uM
4 uM
6 uM
100 nM
I
BO1 CM +
DMSO
JAK1/2i (2 uM)
STAT5i (100 uM)
STAT3i (25 uM)
ERKi (10 uM)
p38i (4 uM)
MEKi (1 uM)
77
0.6
74
4.9
69
0.7
53
43
SSC
EYFP (Arg-1)

Figure 5. GM-CSF signaling regulates myeloid cell Arg-1 expression through non-canonical pathways

(A) Experiment scheme. **(B)** WT or *Stat6*$^{-/-}$ YARG BMMs treated with recombinant IL-4 or PyMT-BO1 tumor cell CM for 24 h, ARG1^{+} cells quantified by FACS. **(C)** *Arg1* mRNA expression in WT and *Stat6*$^{-/-}$ BMMs treated with IL-4 or PyMT-BO1 tumor cell CM (*n*=2 or 3). **(D)** Experiment scheme. **(E, F)** 1x10^{5} PyMT-BO1 tumor cells injected into MFP tissue of WT or *Stat6*$^{-/-}$ YARG mice. After tumor measures 500 mm^{3}, ARG1^{+} cells are quantified by FACS from whole tumor tissue single-cell suspensions (*n*=6). **(G)** Working model of GM-CSF receptor signaling. **(H, I)** ARG1^{+} cells quantified by FACS in YARG BMMs pre-treated with DMSO, JAK1/2 inhibitor Ruxolitinib, STAT3 inhibitor C188-9, STAT5 inhibitor CAS 285986-31-4, ERK1/2 inhibitor Ulixertinib, p38 inhibitor SB203580, and MEK inhibitor Trametinib for 1 h, followed by treatment with BO1 tumor cell CM for 24 h (*n*=2-5). Data are shown as mean ± SEM, **p*<0.05, ***p*<0.01, ****p*≤0.001, using a two-tailed, unpaired *t*-test with Welch's correction.

Figure 6

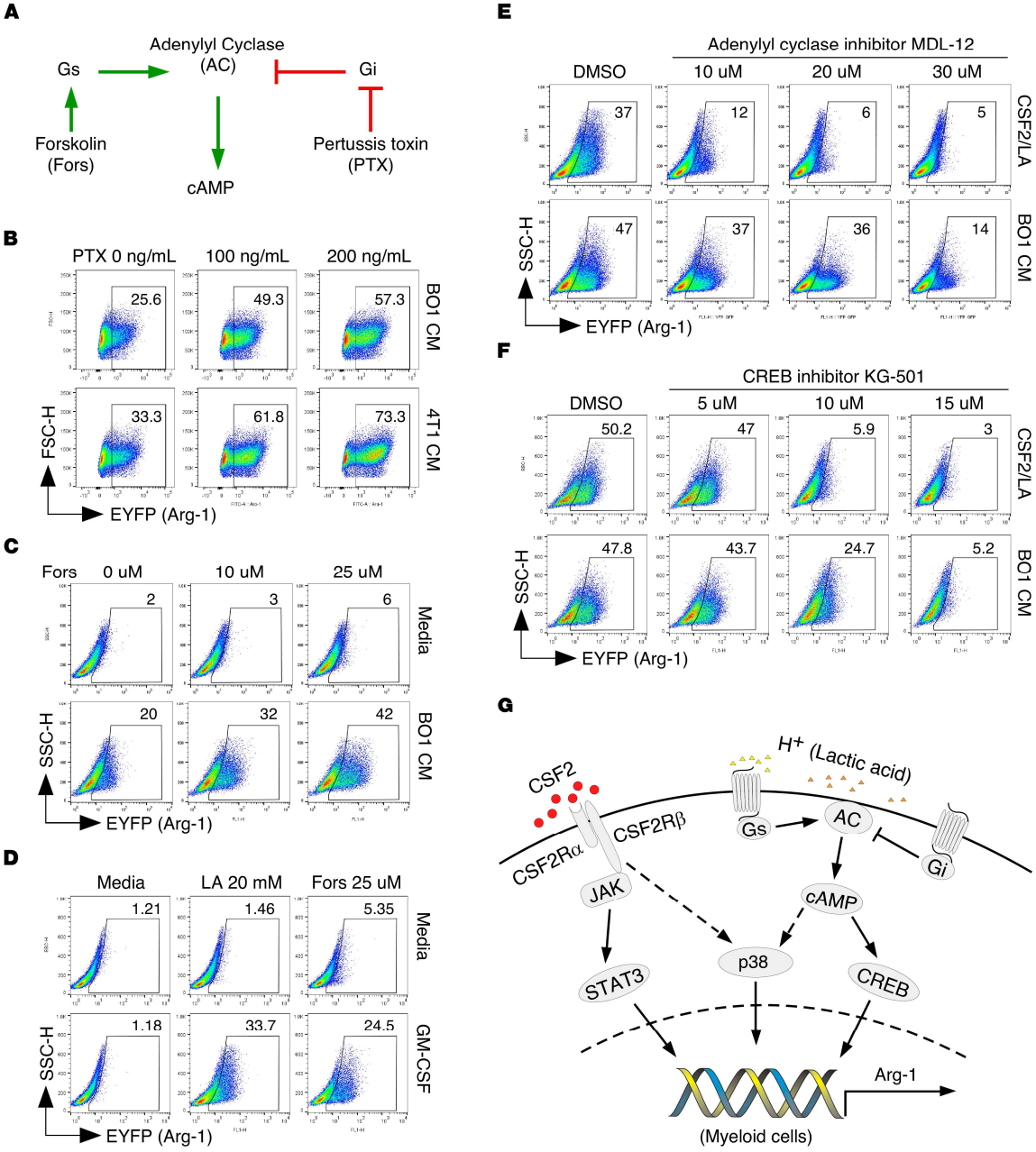
A
Adenylyl Cyclase
(AC)
Gs
Gi
Forskolin
(Fors)
Pertussis toxin
(PTX)
cAMP
B
PTX 0 ng/mL
100 ng/mL
200 ng/mL
25.6
49.3
57.3
33.3
61.8
73.3
BO1 CM
4T1 CM
FSC-H
EYFP (Arg-1)
C
Fors
0 uM
10 uM
25 uM
2
3
6
20
32
42
Media
BO1 CM
SSC-H
EYFP (Arg-1)
D
Media
LA 20 mM
Fors 25 uM
1.21
1.46
5.35
1.18
33.7
24.5
Media
GM-CSF
SSC-H
EYFP (Arg-1)
E
Adenylyl cyclase inhibitor MDL-12
DMSO
10 uM
20 uM
30 uM
37
12
6
5
47
37
36
14
CSF2/LA
BO1 CM
SSC-H
EYFP (Arg-1)
F
CREB inhibitor KG-501
DMSO
5 uM
10 uM
15 uM
50.2
47
5.9
3
47.8
43.7
24.7
5.2
CSF2/LA
BO1 CM
SSC-H
EYFP (Arg-1)
G
H+ (Lactic acid)
CSF2
CSF2Rβ
CSF2Rα
Gs
AC
Gi
JAK
cAMP
p38
STAT3
CREB
Arg-1
(Myeloid cells)

Figure 6. Tumor cell-derived GM-CSF induced myeloid cell Arg-1 expression require cAMP signaling

(A) Working model that G-protein coupled receptors (GPCRs) associated subunit Gs and Gi regulate cAMP level. **(B)** $5x10^5$ BMMs from Arg-1-YFP mice were seeded in 6-well plate overnight. BMMs pre-treated with pertussis toxin (PTX) for 2 h before adding tumor cell CM. **(C, D)** Forskolin (Fors) was added to the BMMs at the same time with indicated treatments. **(E-F)** Inhibitors added 1 h before CM or 2ng/mL GM-CSF plus 20 mM lactic acid (CSF2/LA) treatment. All BMMs were treated for 24 h by CM or CSF2/LA before FACS analysis. In **B-F**, data are representative of three independent experiments. **(G)** A working model that GM-CSF (CSF2) and cAMP signaling combine to induce myeloid cell Arg-1 expression.

Figure 7

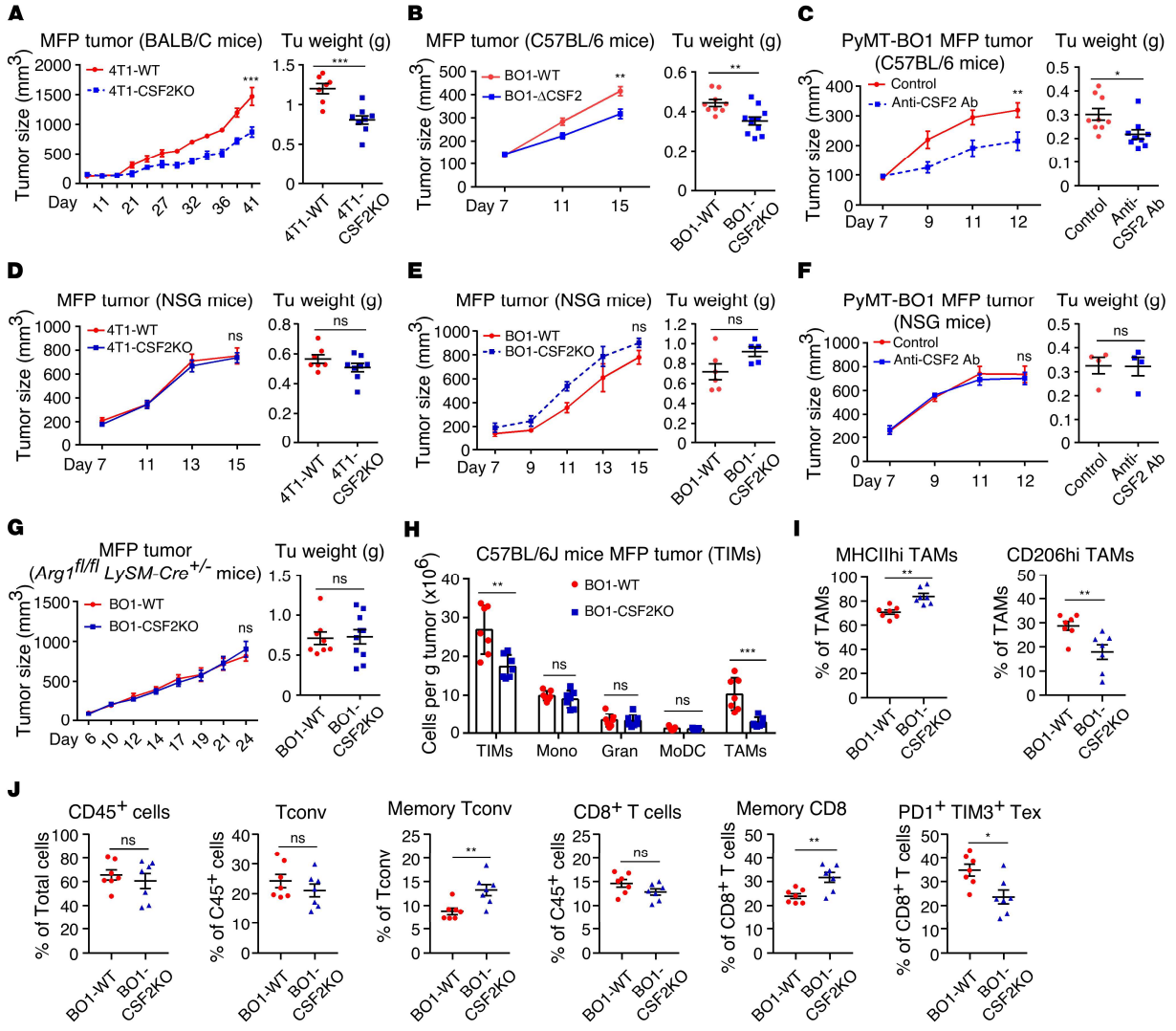
A
MFP tumor (BALB/C mice)
Tu weight (g)
4T1-WT
4T1-CSF2KO
Tumor size (mm3)
Day
4T1-WT
4T1-CSF2KO
B
MFP tumor (C57BL/6 mice)
Tu weight (g)
BO1-WT
BO1-ΔCSF2
C
PyMT-BO1 MFP tumor (C57BL/6 mice)
Tu weight (g)
Control
Anti-CSF2 Ab
D
MFP tumor (NSG mice)
Tu weight (g)
E
MFP tumor (NSG mice)
Tu weight (g)
F
PyMT-BO1 MFP tumor (NSG mice)
Tu weight (g)
G
MFP tumor (Arg1fl/fl LysM-Cre+/- mice)
Tu weight (g)
H
C57BL/6J mice MFP tumor (TIMs)
Cells per g tumor (x10^6)
TIMs
Mono
Gran
MoDC
TAMs
I
MHCIIhi TAMs
CD206hi TAMs
% of TAMs
J
CD45+ cells
Tconv
Memory Tconv
CD8+ T cells
Memory CD8
PD1+ TIM3+ Tex
% of Total cells
% of C45+ cells
% of Tconv
% of CD8+ T cells
ns

Figure 7. Breast tumor-derived GM-CSF promotes tumor growth through the modulation of host immune cells

(A) 1x10^5 4T1-WT (vector control) or 4T1-CSF2 knockout breast tumor cells injected into MFP tissue of 8-week-old female BALB/C mice (*n*=7 or 8). **(B)** 1x10^5 BO1-WT (vector control) or BO1-CSF2 knockout breast tumor cells injected into MFP tissue of 8-week-old female C57BL/6J mice (*n*=9 or 11). **(C)** 1x10^5 BO1-GFP-Luc breast tumor cells mixed with matrigel plus isotype antibody (Control) or anti-CSF2 antibody before injected into MFP tissue of 8-week-old female C57BL/6J mice (*n*=9). **(D-F)** The same experiments in A-C were performed in NSG mice (*n*=4-8). **(G)** The same experiment as (B) was performed in *Arg1*$^{fl/fl}$ *LySM-Cre*$^{+/-}$ mice (*n*=8 or 10). For all the above experiments, tumor growth is measured by digital calipers. At day 24, MFP tumors were dissected and weighed. **(H-J)** Single-cell suspensions from day 10 BO1-WT or BO1-CSF2KO whole tumor tissue (C57BL/6J mice) were analyzed by FACS. Populations of the tumor-infiltrating myeloid cells (TIMs) and T cells are shown (*n*=7). Statistical comparisons by 2-way ANOVA for repeated measures or a two-tailed, unpaired *t*-test with Welch's correction between groups for column data. Data are shown as mean ± SEM, * $p<0.05$, ** $p\leq0.01$, *** $p\leq0.001$.

Figure 8

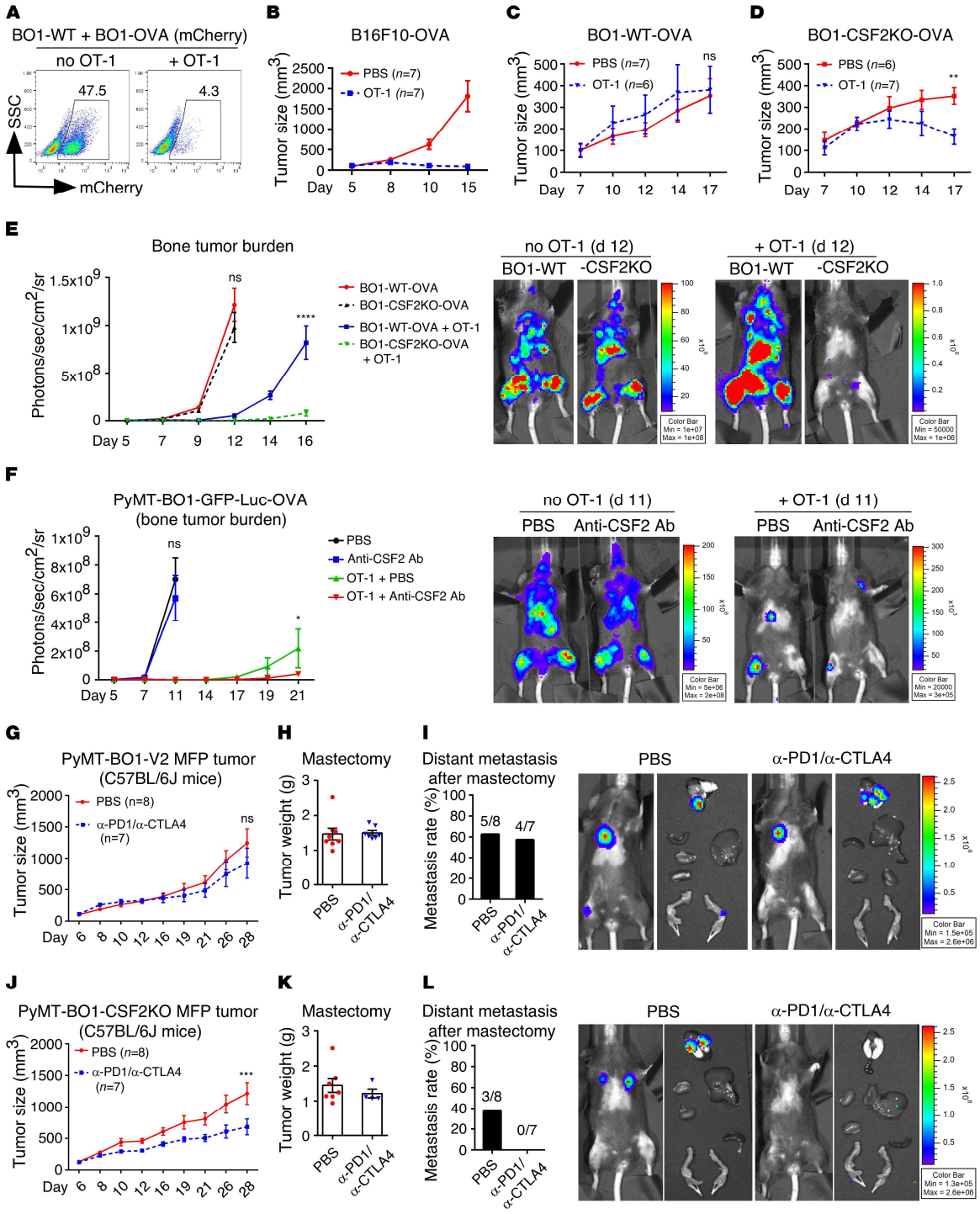
A
BO1-WT + BO1-OVA (mCherry)
no OT-1
+ OT-1
47.5
4.3
SSC
mCherry
B
B16F10-OVA
Tumor size (mm3)
PBS (n=7)
OT-1 (n=7)
Day 5 8 10 15
C
BO1-WT-OVA
PBS (n=7)
OT-1 (n=6)
ns
Day 7 10 12 14 17
D
BO1-CSF2KO-OVA
PBS (n=6)
OT-1 (n=7)
**
Day 7 10 12 14 17
E
Bone tumor burden
Photons/sec/cm2/sr
ns
****
BO1-WT-OVA
BO1-CSF2KO-OVA
BO1-WT-OVA + OT-1
BO1-CSF2KO-OVA + OT-1
Day 5 7 9 12 14 16
no OT-1 (d 12)
+ OT-1 (d 12)
BO1-WT
-CSF2KO
Color Bar Min = 1e+07 Max = 1e+08
Color Bar Min = 50000 Max = 1e+06
F
PyMT-BO1-GFP-Luc-OVA (bone tumor burden)
Photons/sec/cm2/sr
ns
*
PBS
Anti-CSF2 Ab
OT-1 + PBS
OT-1 + Anti-CSF2 Ab
Day 5 7 11 14 17 19 21
no OT-1 (d 11)
+ OT-1 (d 11)
PBS
Anti-CSF2 Ab
Color Bar Min = 5e+06 Max = 2e+08
Color Bar Min = 20000 Max = 3e+05
G
PyMT-BO1-V2 MFP tumor (C57BL/6J mice)
Tumor size (mm3)
PBS (n=8)
α-PD1/α-CTLA4 (n=7)
ns
Day 6 8 10 12 16 19 21 26 28
H
Mastectomy
Tumor weight (g)
PBS
α-PD1/ α-CTLA4
I
Distant metastasis after mastectomy
Metastasis rate (%)
5/8
4/7
PBS
α-PD1/ α-CTLA4
PBS
α-PD1/α-CTLA4
Color Bar Min = 1.5e+05 Max = 2.6e+06
J
PyMT-BO1-CSF2KO MFP tumor (C57BL/6J mice)
Tumor size (mm3)
PBS (n=8)
α-PD1/α-CTLA4 (n=7)
***
Day 6 8 10 12 16 19 21 26 28
K
Mastectomy
Tumor weight (g)
PBS
α-PD1/ α-CTLA4
L
Distant metastasis after mastectomy
Metastasis rate (%)
3/8
0/7
PBS
α-PD1/ α-CTLA4
PBS
α-PD1/α-CTLA4
Color Bar Min = 1.3e+05 Max = 2.6e+06

Figure 8. Disruption of tumor cell produced GM-CSF enhances breast cancer immune therapy
(A) BO1 cells (GFP^+) were co-cultured with BO1-OVA cells (GFP^+ $mCherry^+$) at 1:1 ratio, then OT-1 T cells were added for 16 h and analyzed by FACS. **(B)** $1x10^6$ B16F10-OVA cells were s.c. injected in the C57BL/6j mice. At day 5, one group treated with $5x10^6$ in vitro expanded OT-1 T cells via i.v. injection Tumor size was measured by digital calipers. **(C, D)** $1x10^5$ PyMT-BO1-WT-OVA or PyMT-BO1-CSF2KO-OVA breast tumor cells were inoculated with PBS in MFP tissue. At day 7, $5x10^6$ OT-1 T cells were i.v. injected. **(E)** $1x10^5$ PyMT-BO1-WT-OVA or PyMT-BO1-CSF2KO-OVA breast tumor cells were injected intracardiac into 6-week-old female C57BL/6 mice (*n*= 5 or 6). At day 5, $5x10^6$ OT-1 T cells were injected via i.v. Representative pictures of BLI on day 12 were shown. **(F)** $1x10^5$ PyMT-BO1-OVA breast tumor cells were injected intracardiac into 6-week-old female C57BL/6 mice (*n*= 5 or 6). At day 5, 7, and 11, anti-CSF2 antibody was intravenously injected in antibody treatment groups. At day 5, $5x10^6$ OT-1 T cells injected via i.v. Representative pictures of BLI on day 12 were shown. **(G)** $1x10^5$ PyMT-BO1-V2 breast tumor cells were injected into MFP tissue of 8-week-old female C57BL/6 mice. At day 6, 8, and 10, anti-PD1 and anti-CTLA4 antibodies (2.5mg/kg) were injected by i.v. **(H)** Primary tumor mastectomies were performed when tumor size reached 1200 mm^3. The primary tumor weight after mastectomy is shown. **(I)** After 4 weeks of primary tumor mastectomy, distant metastasis was detected by BLI. The ratio of metastatic events and representative pictures of BLI are shown. **(J-L)** The same experiments were performed using PyMT-BO1-CSF2KO breast tumor cells. Statistical comparisons by 2-way ANOVA. Data are shown as mean ± SEM, *$p \leq 0.05$, **$p \leq 0.01$, ***$p \leq 0.001$, ****$p \leq 0.0001$.